

High-velocity clouds as streams of ionized and neutral gas in the halo of the Milky Way^{*}

N. Lehner^{1†}, J. C. Howk¹, C. Thom², A. J. Fox², J. Tumlinson², T. M. Tripp³, and J. D. Meiring³

¹*Department of Physics, University of Notre Dame, Notre Dame, IN 46556, USA*

²*Space Telescope Science Institute, Baltimore, MD 21218, USA*

³*Department of Astronomy, University of Massachusetts, Amherst, MA 01003, USA*

Accepted XXX. Received XXX; in original form XXX

ABSTRACT

High-velocity clouds (HVC), fast-moving ionized and neutral gas clouds found at high galactic latitudes, may play an important role in the evolution of the Milky Way. The extent of this role depends sensitively on their distances and total sky covering factor. We search for HVC absorption in *Hubble Space Telescope* high resolution ultraviolet spectra of a carefully selected sample of 133 AGN using a range of atomic species in different ionization stages (e.g., O I, C II, C IV, Si II, Si III, Si IV). This allows us to identify neutral, weakly ionized, or highly ionized HVCs over several decades in H I column densities. The sky covering factor of UV-selected HVCs with $|v_{\text{LSR}}| \geq 90$ km s^{−1} is $68\% \pm 4\%$ for the entire Galactic sky. About 74% of the HVC directions have $N(\text{H I}) < 3 \times 10^{18}$ cm^{−2} and 46% have $N(\text{H I}) < 8 \times 10^{17}$ cm^{−2}. We show that our survey is essentially complete, i.e., an undetected population of HVCs with extremely low H (H I+H II) column density is unlikely to be important for the HVC mass budget. We confirm that the predominantly ionized HVCs contain at least as much mass as the traditional H I HVCs and show that large H I HVC complexes have generally ionized envelopes extending far from the H I contours. There are also large regions of the Galactic sky that are covered with ionized high-velocity gas with little H I emission nearby. We show that the covering factors of HVCs with $90 \leq |v_{\text{LSR}}| \lesssim 170$ km s^{−1} drawn from the AGN and stellar samples are similar. This confirms that these HVCs are within 5–15 kpc of the sun. The covering factor of these HVCs drops with decreasing vertical height, which is consistent with HVCs being decelerated or disrupted as they fall to the Milky Way disk. The HVCs with $|v_{\text{LSR}}| \gtrsim 170$ km s^{−1} are largely associated with the Magellanic Stream at $b < 0^\circ$ and its leading arm at $b > 0^\circ$ as well as other large known H I complexes. Therefore there is no evidence in the Local Group that any galaxy shows a population of HVCs extending much farther away than 50 kpc from its host, except possibly for those tracing remnants of galaxy interaction.

Key words: Galaxy: halo – Galaxy: evolution – Galaxy: structure

1 INTRODUCTION

The ability of galaxies to form stars depends sensitively on the content and physical conditions of their gas, which in turn is dictated by internal effects, such as feedback, as well as by the external interaction of galaxies with their

surroundings. A galaxy may exchange mass with its circumgalactic environment through the infall of intergalactic matter or of remnants resulting from galaxy interactions, and through the outflows driven by stellar and AGN feedback. Despite many theoretical and observational efforts (a non exhaustive list of references includes Oort 1970; Steidel & Sargent 1992; Kereš et al. 2005; Bouché et al. 2007; Peek et al. 2008; Dekel et al. 2009; Prochaska & Hennawi 2009; Oppenheimer et al. 2010; Fumagalli et al. 2011; Marinacci et al. 2011; Tripp et al. 2011; Tumlinson et al. 2011), the cycle of baryons in and out of galaxies and its implications

^{*} Based on observations made with the NASA/ESA Hubble Space Telescope, obtained at the Space Telescope Science Institute, which is operated by the Association of Universities for Research in Astronomy, Inc. under NASA contract No. NAS5-26555.
[†] e-mail: N.Lehner@nd.edu

for galaxy evolution are not yet fully understood. This exchange of baryons between galaxies and their environments must, however, result in a net gain of mass if galaxies are to form stars over many billions of years.

In our own Milky Way, it has been long known that there must be streams or flows of gas through the Galactic halo. Signatures of these flows are revealed by the high-velocity clouds (HVCs), clouds moving in the local standard of rest (LSR) frame at $|v_{\text{LSR}}| \geq 90 \text{ km s}^{-1}$ (Wakker & van Woerden 1997). The unknown distances to these clouds for a long time meant we did not know if the HVCs were associated with streams occurring near the Milky Way (e.g., Oort 1970) rather than the IGM of the Local Group (e.g., Blitz et al. 1999; Gnat & Sternberg 2004). Furthermore, the distances to the HVCs are required for quantifying their basic physical properties (several scale with the distance, e.g., the mass $M \propto d^2$). Since the last large summary on the distances and metallicities of the H I HVCs published 10 years ago (Wakker 2001), our knowledge of these clouds has dramatically improved. Distances of several individual large HVC complexes seen in H I emission are now determined, placing them at heliocentric distances of about 4–15 kpc (e.g., Ryans et al. 1997; Wakker 2001; Thom et al. 2006, 2008; Wakker et al. 2007, 2008; Lehner & Howk 2010; Smoker et al. 2011). Among the large complexes (in terms of mass and solid angle), only the Magellanic Stream (e.g., Putman et al. 1998; Brüns et al. 2005; Nidever et al. 2008) is much farther away, possibly extending to 80–200 kpc according to recent numerical models of the interaction of the Large and Small Magellanic Clouds (Besla et al. 2012).

With the advent of sensitive high resolution UV spectrographs including the *Far Ultraviolet Spectroscopic Explorer (FUSE)* and those of the *Hubble Space Telescope (HST)*, it has also become obvious that HVCs are both neutral and ionized in view of the high-velocity absorption detected in resonance lines of neutral, weakly ionized, and highly ionized species in the spectra of AGN (e.g., Sembach et al. 1995, 1999, 2000; Savage et al. 2000; Lehner et al. 2001; Sembach et al. 2003; Wakker et al. 2003; Collins et al. 2005; Fox et al. 2006; Shull et al. 2009; Richter et al. 2009; Tripp & Song 2012). The importance of ionized gas can be demonstrated simply by considering the fraction of the sky covered by HVCs at H I column sensitivities. While only 18% is covered at a sensitivity of $\log N(\text{H I}) \gtrsim 18.5$ (Wakker 1991), a limit easily detected in H I 21 cm observations, deeper H I emission observations ($\log N(\text{H I}) \gtrsim 17.9$) yield a factor larger covering factor, 37% (Murphy et al. 1995; Lockman et al. 2002). A much larger fraction of the sky is even covered by the HVCs seen in absorption, which are sensitive to much lower $N(\text{H I})$: for the HVCs with O VI absorption, the HVC covering factor is about 60–75% (Sembach et al. 2003; Fox et al. 2006), and a high covering factor was also found for the HVCs detected via the strong line of Si III (Shull et al. 2009; Collins et al. 2009, hereafter CSG09).

Many of these HVCs observed in absorption have been often dubbed as ionized HVCs or highly ionized HVCs since in many cases a large fraction of the gas is photoionized or collisionally ionized, i.e., $N(\text{H II}) \gg N(\text{H I})$. In this work, we simply label them as HVCs. To differentiate them from the HVCs observed in H I emission, we refer to the latter category as H I HVCs. We emphasize that the only real distinction with this definition is that the H I HVCs are

detectable via 21-cm emission. Thus they have a clear H I sensitivity cut-off determined by the depth of the observations and limitation of radio emission studies. On the other hand, for the HVCs (i.e., those seen in UV absorption), the amount of H I can vary greatly as demonstrated by the observed range in the H I column density: $N(\text{H I}) \lesssim 10^{15} \text{ cm}^{-2}$ to $N(\text{H I}) \gtrsim 10^{20} \text{ cm}^{-2}$ derived from Lyman series absorption (Fox et al. 2006; Zech et al. 2008) and H I 21-cm emission observations toward the AGN; virtually *any* $N(\text{H I})$ column densities are observed in the UV-selected HVC. However, even if the H I column density can be small, the total H (H I+H II) column density of the HVCs can still be substantial, $\gtrsim 10^{17}\text{--}10^{18} (Z/Z_{\odot})^{-1} \text{ cm}^{-2}$ on average (e.g., Sembach et al. 2003; Shull et al. 2009). As for the H I HVCs, direct distance constraints are required for determining the masses of the HVCs seen in UV absorption and for characterizing their role in the evolution of the Milky Way and their relationship with the H I HVC complexes. If they are in the Milky Way within several kpc, the HVCs seen in UV absorption are not only more important in number and mass, but their relative proximity may allow them to descend into the disk to fuel new generations of star formation (e.g., Shull et al. 2009; Lehner & Howk 2011).

Lehner & Howk (2011, hereafter LH11) ruled out whole classes of HVCs using a novel and powerful method to statistically constrain the distance of the entire HVC population rather than just a few individual clouds. This was done by comparing the UV absorption line detection rates of HVCs in COS and STIS spectra of stars (distance limited) and AGN (no distance limit). They selected 28 stars (hereafter, the LH11 stellar sample) to be at the largest practical distances in order to distinguish between Milky Way halo and Local Group origins for the HVCs, resulting in targets at $|z| \gtrsim 3$ kpc from the Galactic plane and heliocentric distances $3 \leq d \leq 32$ kpc (although most of the stars are within $\langle d \rangle = 11.6 \pm 6.9$ kpc). The stellar sightlines were carefully selected to be well distributed across the high latitude Galactic sky and avoid biases that *a priori* favor or disfavor the presence of HVCs along each sightline. They identified HVC absorption in the stellar spectra using the strongest lines of atomic, singly, and doubly ionized species available in the UV bandwidth (e.g., C II $\lambda 1334$, C IV $\lambda 1548$, Si II $\lambda 1260$, Si III $\lambda 1206$, O I $\lambda 1302$), most showing high [Si II/O I] ratio, consistent with these HVCs being mostly ionized. The HVC sky covering factors of the HVCs with $90 \leq |v_{\text{LSR}}| \lesssim 170 \text{ km s}^{-1}$ determined from the stellar and AGN samples are $f_c \simeq 0.50$ and $\lesssim 0.65$, respectively (LH11). Unfortunately the HVC covering factor for the AGN sample suffers from poorly understood selection criteria, resulting only in an upper limit on f_c . Nevertheless the similarity in the covering factors between the distance limited sample and the sample with no distance limit imply that most of the HVCs with $90 \leq |v_{\text{LSR}}| \lesssim 170 \text{ km s}^{-1}$ are within heliocentric distances 5–15 kpc (no HVC at $|v_{\text{LSR}}| \gtrsim 200 \text{ km s}^{-1}$ was found in the stellar sample). Given the importance of HVC distances and the importance of the covering factor in determining d , one of our goals here is to robustly determine the covering factor of the HVCs from a well understood sample of AGN that can be directly compared to the LH11 stellar sample. To search for the HVCs, we do not focus on a single ion, but on a suite of atoms and ions (e.g., O I, C II, C IV,

Si II, Si III, Si IV, Al II) following the same method used by LH11. This allows us not only to securely detect HVC absorption, but also, as we will show, to sensitively search for HVCs at all levels of ionization.

Here we present the results of our new study of HVCs, with the following organization. In §2 we describe our samples of AGN, the data and their sensitivity, and the method for determining the presence of HVCs. In §3 we present our findings for the covering factors of the HVCs and VHVCs. With this new sample of AGN, we strengthen the LH11 results, and we extend their results by using stars at smaller distances to study the dependence between the covering factor and the distance. With our much larger sample of AGN and much better sky coverage than the sample used in LH11, we are also able to gain insight into the origins and distances of the very high-velocity clouds (VHVCs, $|v_{\text{LSR}}| \gtrsim 170 \text{ km s}^{-1}$). In §4 we connect the HVCs detected in H I emission and UV absorption based on their closed proximity on the sky, in velocity, and in space (distance). We discuss some of the implications of our results for the mass of the HVCs and their origins and fate in §5. Finally, we present a summary in §6.

2 AGN SAMPLE AND DATA

2.1 Description of the main AGN sample

The 67 AGN in our main sample were drawn from 3 *HST*/COS large programs: 11598 (“How Galaxies Acquire their Gas: A Map of Multiphase Accretion and Feedback in Gaseous Galaxy Halos”, PI: Tumlinson), 11741 (“Probing Warm-Hot Intergalactic Gas at $0.5 < z < 1.3$ with a Blind Survey for O VI, Ne VIII, Mg X, and Si XII Absorption Systems, PI: Tripp), and 12248 (“How Dwarf Galaxies Got That Way: Mapping Multiphase Gaseous Halos and Galactic Winds Below L^* ”, PI: Tumlinson).¹ The aims of these 3 programs are to target science beyond the Milky Way halo. Therefore the choice of the targets was completely random with respect to the locations of the H I HVCs. Hereafter we refer to this sample as the TT (Tripp–Tumlinson) sample.

Information on the design and performance of COS can be found in Green et al. (2012). The data reduction and co-addition procedures are described in Thom et al. (2011) and Meiring et al. (2011), and we refer the reader to these papers for more details on data processing. Notably the individual exposures were co-added in photon counts, rather than flux calibrated exposures. The shifts between the individual exposures were determined using the Galactic interstellar absorption lines. The exposures were shifted to a common reference and co-added. All the data were then shifted to the local standard of rest (LSR) frame. A visual comparison between the Galactic H I emission spectra from the Leiden/Argentine/Bonn (LAB) survey (Kalberla et al. 2005) and the Galactic absorption indicates that the spectra were correctly shifted in the absolute LSR frame. The COS resolution of the G130M and G160M gratings is $R \approx 17,000$, which is adequate for identifying HVCs (Lehner & Howk 2010, LH11). The typical signal-to-noise of the co-added

spectra are about 4–9, > 20 , and 9–13 per resolution element for programs 11598, 11741, and 12248, respectively. A few sightlines were not considered in the programs 11598 and 12248 owing to the poor signal-to-noise of their spectra ($\lesssim 3$) or excessive contamination from higher redshift absorbers.

In Fig. 1, we show the sky distribution of the 67 TT targets, and in Table 1 we list their Galactic coordinates. Most of the targets are situated in the northern Galactic hemisphere as the two largest samples (11598 and 12248) were selected from the Sloan Digital Sky Survey (SDSS). There is an excellent coverage of the Galactic sky in longitude and $b \gtrsim 30^\circ$. There is also good overall agreement in the sky coverage between the TT sample and sample of stars assembled by LH11 as demonstrated in Fig. 1.

2.2 Additional sample of AGN

In order to achieve the best sky coverage possible, we also consider two additional samples: 1) 18 publicly available COS AGN spectra from the Guaranteed Time Observer (GTO) IGM program, and 2) 49 AGNs drawn from the STIS E140M and G140M AGN sample from CSG09.

The GTO COS spectra were reduced following the procedure described in §2.1. We only considered AGN that were initially targeted for IGM science, not the AGN from the GTO Galactic–HVC program to avoid obvious selection bias. The GTO sample is summarized in Table 2.

The only explicit two criteria for selecting sightlines in CSG09 were that 1) $S/N \geq 3$, and 2) little apparent contamination from the QSO absorbers. However, we need to remove any potential bias from their sample, as, e.g., some of their AGN were initially targeted for HVC science (with a priori knowledge from past observations that an HVC was along the line of sight). In order to identify AGN originally targeted for HVC science, we reviewed the MAST program abstract and title for each target in CSG09 and found that 7 sightlines were explicitly selected to study HVCs. Those were not considered further. From the appendix in CSG09, we determined that 6 lines of sight had an HVC detection solely based on Si III absorption (for the other HVCs, they have confirmation of the absorption using several species and/or transitions, i.e., consistent with our criteria from §2.3). This differs from our method in which we only classify an HVC detection based on its detected absorption in more than one species. Considering these sightlines but classifying them with no HVC detection or removing these sightlines from the counting would not change the results appreciably. We include these sightlines but do not count them as detections (see next in §2.3).

2.3 Search for HVC absorption

In order to search for the high-velocity interstellar absorption ($90 \leq |v_{\text{LSR}}| \leq 400 \text{ km s}^{-1}$) in the TT and GTO samples, we first used the strongest lines of atomic, singly, and doubly ionized species available in the COS UV bandwidth: C II $\lambda 1334$ ($f\lambda = 171$), Si II $\lambda 1260$ ($f\lambda = 1487$), and Si III $\lambda 1206$ ($f\lambda = 1967$). The smaller $f\lambda$ for C II is compensated by the fact that C is about 8 times more abundant than Si in a standard solar abundance pattern. These ions have been

¹ The program 12248 is not completed yet; only data taken prior to November 2011 are in this paper.

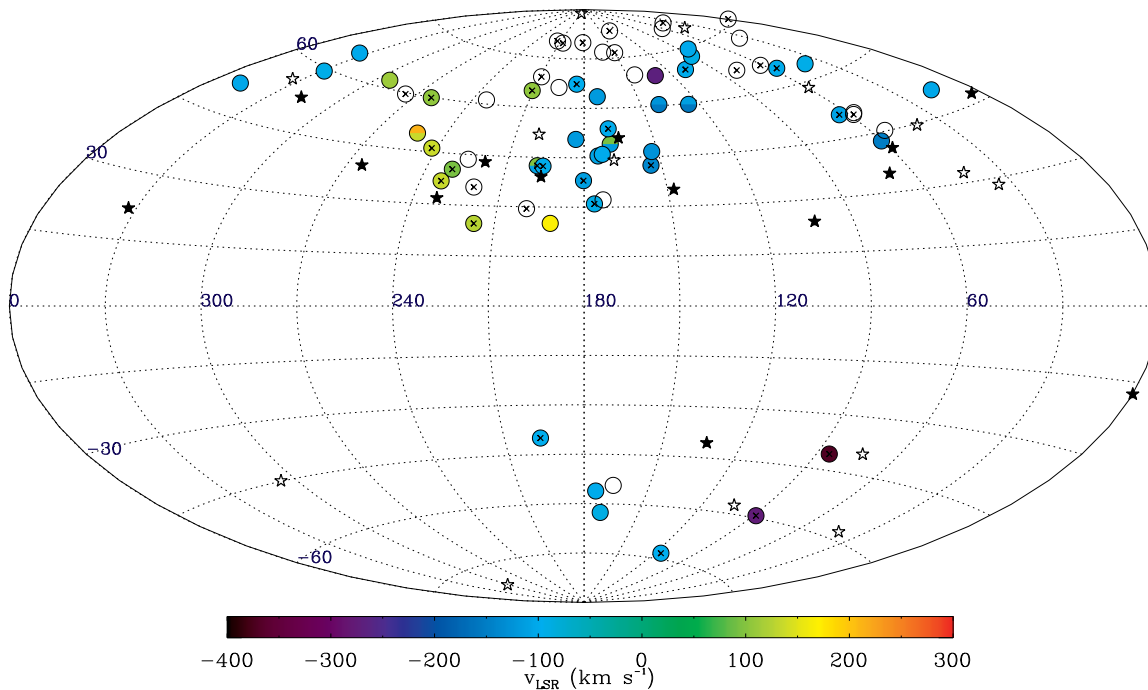


Figure 1. Aitoff projection map of the survey directions for the TT sample. Sightlines are plotted in Galactic coordinates with longitude increasing from right to left. A colored circle indicates an HVC along the line of sight while open circle implies no HVC along the sightline. Circles with a cross indicate that the sightline is part of the high-sensitivity sample with $10 \leq W_{\text{lim}} \leq 42$ mÅ. The velocity value is color coded following the horizontal color bar. The star symbol shows the positions of the stars from the sample of LH11 where a filled symbol indicates that an HVC is detected in the foreground of the stars, while an open symbol shows the absence of HVC along the stellar sightline.

shown to be extremely powerful for finding low H I column density HVCs, and more precisely HVCs with virtually any H I column densities (see below). The use of multiple transitions is crucial when using high redshift AGN because the likelihood of unrelated QSO absorber contamination is not negligible. Our rule is that an HVC absorption is defined as such only if it is seen in absorption in at least two species or atomic transitions. The same rule was used by LH11 for their stellar sample. To confirm the detection or to help determine the velocity of the HVCs, we also used tracers of neutral gas (e.g., O I), weaker transitions of Si II, and tracers of more highly ionized gas (e.g., C IV). The strong line of the C IV doublet has $f\lambda = 147$, comparable to the strength of C II, but C IV is more suitable than C II if the gas is highly ionized. In Fig 2, we show four sightlines from the TT sample, highlighting the diversity of UV-selected HVCs. The absorption profiles in this figure were normalized using Legendre polynomials with degrees $d \leq 3$.

Fig. 2 shows that specific examples that the ionization conditions change from sightline to sightline with in some cases only the detection of C II, Si III, and Si III (no high ion), and in other cases only detection of Si III and C IV (no low ion). To illustrate this change in the ionization conditions, we show in Fig. 3 a Cloudy (Ferland et al. 1998) photoionization model that predicts the column densities of H I, C II, C IV, Si II, Si III, and Si IV as a function of ionization parameter ($U = n_\gamma/n_H$, where n_γ and n_H are the densities of ionizing photons and hydrogen). The radiation field is from the combined Milky Way and UV background radiation fields

at a Galactocentric radius (R_G) of 10 kpc and a z -height of 5 kpc (Fox et al. 2005, 2010). These distances were chosen because they are close to the observed values of the HVCs (this paper, LH11, Thom et al. 2006, 2008; Wakker et al. 2008, 2007). We consider a total H column density of 10^{19} cm $^{-2}$ and a metallicity of a 1/3 solar (see §5.1). It is evident from this figure that the combination of several ions of the same and different species is extremely powerful for finding HVCs; e.g., as U increases, the amount of C II diminishes and may become undetectable, but then C IV can be detected. Therefore the available UV diagnostics allow us to search sensitively for any types of HVCs, neutral, weakly, or highly ionized, and this is well illustrated in Fig. 2. Also note that the H I column density decreases by a large amount from about 10^{19} to 10^{15} cm $^{-2}$ for $-5 \leq \log U \leq -1$. The total H column density is by definition always 10^{19} cm $^{-2}$ in this illustration.

The fourth column of Table 1 summarizes the detection or non-detection of HVCs along the sight lines of the TT sample, including the velocity of detected HVC absorption. The velocities listed in this table were estimated from the apparent optical depth-weighted mean velocity $\langle v \rangle = \int v \tau_a(v) dv / \int \tau_a(v) dv$. A colon in this column highlights that the velocity is severely blended with the lower velocity gas. A velocity with the superscript c indicates that the HVC was only detected in Si III and C IV; there are only 5 such cases.

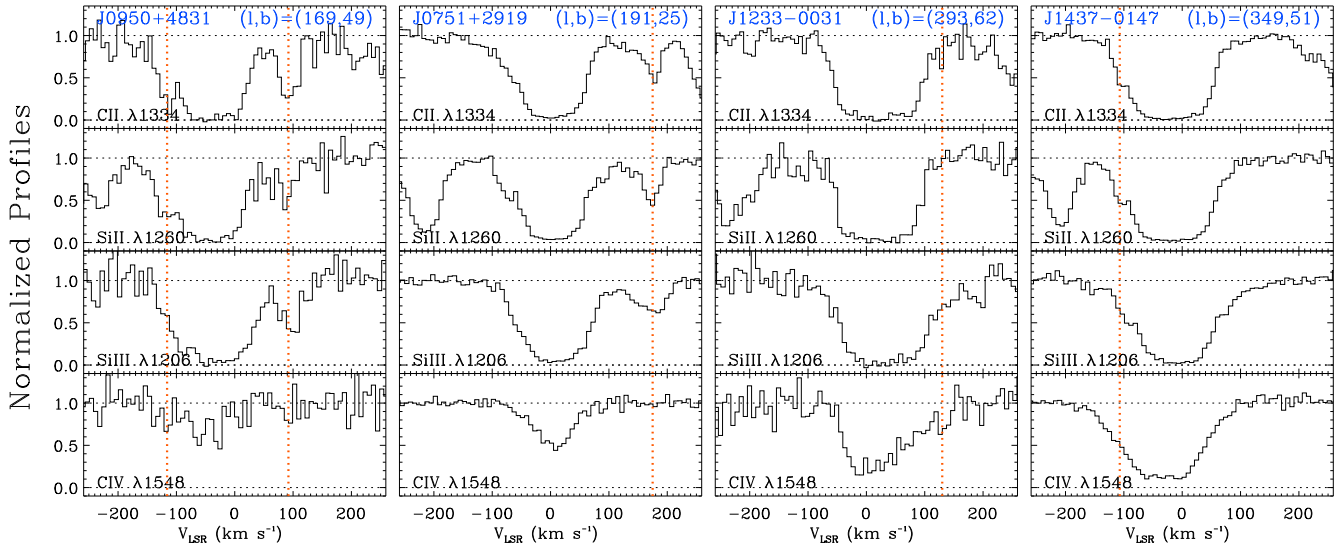


Figure 2. Examples from the TT sample showing the variety of HVCs and S/N. The dotted vertical lines show the HVC detections. The only sightline that passes through an H I HVC complex (A) is J0950+4831, but only the negative component is associated with complex A along this direction. There is no H I HVC complex near the other directions (however, while complex L is several degrees away from J1437-0147, it has similar LSR velocities as seen toward this sightline). Also note how the ionization conditions can change with, e.g., in some cases absorption only in singly and doubly ionized species (J0751+2919) and in other cases only in doubly and triply ionized species (J1233-0031).

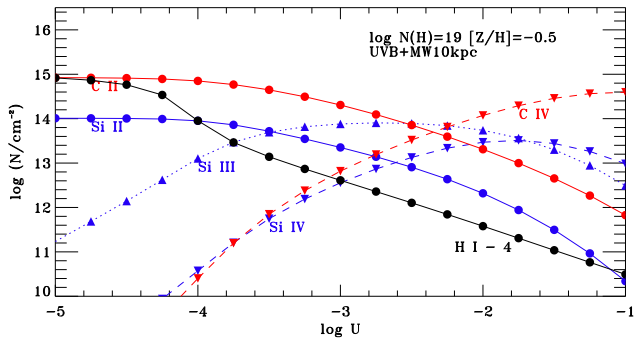


Figure 3. Cloudy simulations predicting the column density of the observed ions against the ionization parameter $U = n_e/n_H$. The radiation field is from the combined, Milky Way plus UV background radiation field at the position $R_G = 10$ kpc and $z = 5$ kpc. Note that in this Cloudy simulation $N(H)$ is fixed and $N(H I)$ varies.

2.4 Sensitivity

Knowing the sensitivity of our sample is key for determining if the detection of the HVC is dependent on the S/N of the spectra and for comparing or combining our sample with other samples. Below we demonstrate that the TT sample is sensitive enough to detect HVC absorption at a level previously detected in other samples.

2.4.1 Sensitivity of the TT sample

In Table 1, we report the 3σ upper limits on the equivalent width (W_{lim}) obtainable for each line of sight from the TT sample and display its distribution in Fig. 4. We estimated W_{lim} near the Si III absorption, but the distribution of W_{lim}

near C II or Si II would be very similar (although the actual value of W_{lim} of C II or Si II may be different from those listed in Table 1 for a given sightline). To estimate W_{lim} , we measured the equivalent width (and 1σ error) over the same velocity range ($\sim 80 \text{ km s}^{-1}$) that is usually observed when an HVC is detected. The 3σ upper limit on the equivalent width is defined as the 1σ error times three. The mean and median of W_{lim} are 42 mÅ , and the dispersion around of the mean is $\sigma_d = 16 \text{ mÅ}$. Assuming the absorption line lies on the linear part of the curve of the growth, $\langle W_{lim} \rangle$ corresponds to $\log N(\text{C II } \lambda 1334) \sim 13.3$, $\log N(\text{C IV } \lambda 1548) \sim 13.0$, $\log N(\text{Si II } \lambda 1260) \sim 12.4$, $\log N(\text{Si III } \lambda 1206) \sim 12.3$.

2.4.2 Comparison with previous samples of detected HVCs

In order to compare our results with others, we estimated the equivalent widths W_λ of C II for the HVC component when it is detected. We chose C II because this ion is cleanly observed in the stellar spectra. For example, in stellar spectra, Si III $\lambda 1206$ cannot always be estimated owing to contamination by the star itself or because the blended interstellar and stellar Ly α absorption can severely depress the flux near Si III. We did not attempt to separate severely blended HVC components and only measured W_λ when the HVC absorption was not entirely blended with the lower velocity absorption. In Fig. 4, we show the distribution of $W_\lambda(\text{C II})$ in the TT sample. The strength of most of the detected HVC absorption features is above $\langle W_{lim} \rangle + 2\sigma_d$ and is strictly larger than $\langle W_{lim} \rangle$.

Using the stellar sample of LH11, we similarly estimated $W_\lambda(\text{C II})$ when a HVC is detected. Although the average S/N of the stellar spectra is higher than the S/N of the AGN spectra in the TT sample, the equivalent widths of HVCs in the stellar sample are such that $W_\lambda \gtrsim \langle W_{lim} \rangle + 2\sigma_d$ (see Fig. 4). This implies that the detection rates of the

Table 1. The AGN sample

Name	l ($^{\circ}$)	b ($^{\circ}$)	$v_{\text{LSR}}^{\text{HVC}}$ (km s^{-1})	W_{lim}^a (m\AA)	P^b
J1342+1844	0.13	+75.48	...	47.7	2
J1524+0958	14.89	+50.12	−106	19.1	3
J1409+2618	34.67	+72.59	...	10.0	3
J1451+2709	39.62	+63.43	−95 :	41.4	2
J1330+2813	42.37	+81.23	...	42.1	1
J1619+3342	54.59	+45.18	...	30.7	1
J1445+3428	56.74	+64.59	−101	47.9	1
J1553+3548	57.26	+50.67	...	40.4	1
J1555+3628	58.32	+50.27	...	49.7	1
J1632+3737	60.34	+42.94	−152	9.5	3
J1330+3119	61.27	+80.41	...	36.7	2
J1435+3604	61.52	+66.26	...	60.2	1
J1550+4001	63.96	+50.94	−108	81.1	1
J1419+4207	78.58	+66.66	...	52.8	1
J1342+3829	83.11	+74.40	−102	27.3	2
J2257+1340	85.28	−40.73	−370	64.6	1
J2345−0059	88.79	−59.39	−276	48.5	1
J1341+4123	90.59	+72.48	−93	27.0	3
J1322+4645	107.71	+69.44	−100 :	47.0	1
J0042−1037	115.13	−73.36	−98	53.4	1
J1241+5721	125.48	+59.73	−158, −113	37.0	1
J1233+4758	131.24	+68.87	−270	37.7	1
J1245+3356	133.72	+83.06	...	48.2	1
J1151+5437	140.61	+60.39	−155, −126 :	12.0	3
J1208+4540	144.63	+69.62	...	14.4	3
J1220+3853	149.71	+76.59	...	61.5	1
J1001+5944	152.44	+46.53	−128	31.1	2
J0928+6025	154.10	+42.44	−141	70.6	1
J1211+3657	161.27	+76.95	...	36.0	2
J0226+0015	166.57	−54.38	...	37.1	1
J0950+4831	168.96	+49.10	−116, +92	40.0	1
J1016+4706	169.03	+53.74	−100	43.9	1
J0212−0737	171.06	−62.64	−91 :	29.2	2
J1103+4141	172.52	+63.52	−120	44.2	2
J0929+4644	172.65	+46.02	−100 :	25.9	2
J0809+4619	173.33	+32.21	...	31.4	2
J0925+4535	174.42	+45.54	−108	29.9	2
J0235−0402	174.46	−56.16	−100	23.3	3
J0803+4332	176.40	+31.00	−95 ^c	57.2	1
J0843+4117	180.21	+38.06	−114	59.2	2
J1210+3157	181.58	+79.96	...	55.9	2
J0949+3902	183.55	+50.57	−120	37.9	2
J1112+3539	184.71	+67.34	−99 ^c	59.5	1
J0751+2919	191.34	+25.05	+175	13.5	3
J1104+3141	195.45	+66.24	...	41.1	2
J0912+2957	195.86	+42.34	−100 :	71.5	2
J0401−0540	196.42	−39.97	−99 :	52.8	1
J0914+2823	198.13	+42.45	−110 :, +95 :	47.2	1
J0820+2334	199.80	+29.42	...	42.0	1
J1204+2754	206.11	+79.62	...	45.4	2
J1117+2634	209.19	+69.21	...	45.9	2
J1059+2517	210.82	+64.96	+102 ^c	46.0	2
J1207+2624	214.56	+80.11	...	51.4	2
J0826+0742	216.89	+24.66	+125	46.5	2
J0910+1014	219.82	+35.48	...	94.0	1
J0947+1005	225.59	+43.59	...	36.4	2
J0943+0531	230.04	+40.41	+90	55.9	1
J0935+0204	232.39	+36.84	+132	55.4	1
J1059+1441	232.72	+61.19	...	37.2	2
J1022+0132	242.16	+46.07	+135	55.3	1
J1051−0051	252.24	+49.88	+131, +210	37.8	2
J1133+0327	261.35	+59.87	+102	52.3	1
J1157−0022	275.71	+59.64	...	49.2	1
J1233−0031	293.11	+61.99	+130 : ^c	29.0	1
J1342−0053	328.82	+59.37	−95	35.6	1
J1342+0505	333.75	+64.84	−103 ^c	38.0	2
J1437−0147	348.72	+51.37	−107	15.4	3

Note: Absence of value in the velocity column indicates that there is no evidence of HVC along the line of sight. Uncertainty in the velocity is dominated by the COS wavelength calibrations, yielding an error of $\sim 10 \text{ km s}^{-1}$; the statistical error is generally $< 3 \text{ km s}^{-1}$, except for those marked with a colon. A velocity value followed by a colon is uncertain owing to blending with the lower velocity gas.

(a): 3σ equivalent width detection limits. We estimated W_{lim} near the Si III absorption, but the distribution of W_{lim} for C II or Si II would be very similar (although the actual value of W_{lim} of C II or Si II may be different for a given sightline; see §2.4). (b): *HST* Program: (1) 11598, (2) 12248, (3) 11741. (c) HVC only detected in Si III and C IV (not Si II or C II).

Table 2. The GTO IGM sample

Name	l ($^{\circ}$)	b ($^{\circ}$)	$v_{\text{LSR}}^{\text{HVC}}$ (km s^{-1})
1ES1553+113	21.91	+43.96	...
PG1259+593	120.56	+58.05	−142
SBS1122+594	141.80	+54.71	−95
VIIIZW244	136.66	+32.67	−93
3C263	134.16	+49.74	−166, −122
PG1115+407	172.23	+66.67	−110 :
MRK421	179.83	+65.03	−119
HS1102+3441	188.56	+66.22	...
TON580	194.94	+72.03	...
HE0238−1904	200.48	−63.63	...
PKS0405−123	204.93	−41.76	+110
HE0226−4110	253.94	−65.78	+156, +208
HE0435−5304	261.02	−41.38	+100 :
HE0439−5254	260.69	−40.90	+106, +300
RXJ0439.6−5311	261.22	−40.93	+116, +300
HE0153−4520	271.80	−67.98	+110, +197
PKS2005−489	350.37	−32.60	...
RXJ2154.1−4414	355.18	−50.87	...

Note: A velocity value followed by a colon is uncertain owing to blending with the lower velocity gas.

stellar and AGN TT samples can be directly compared as we observe no HVC with $W_{\lambda} < \langle W_{\text{lim}} \rangle + 2\sigma_d$.

Several AGN in CSG09 have spectra with S/N similar to the average S/N in the TT sample, but several of them have also higher S/N (see Figs. 1 and 2 in CSG09). In Fig. 4, we show the measured Si III equivalent widths by CSG09 in the individual components of the HVCs of their sample. Following our guidelines, we removed any HVC that is identified only with Si III. Except for 3 high-velocity components, all the detected HVCs in CSG09 have also an equivalent width larger than $\langle W_{\text{lim}} \rangle$. Another way to consider the CSG09 sample is for each sightline to retain only the strongest HVC absorption components. This is shown by the black histogram in Fig. 4. For either samples, we find that most of the detected HVC absorption features have $W_{\lambda} > \langle W_{\text{lim}} \rangle + 2\sigma$ and is larger than $\langle W_{\text{lim}} \rangle$.

The sensitivity of the GTO sample is typically similar to the best S/N in the TT sample (i.e., comparable to data in the GO program 11741). Yet, we estimate equivalent widths of the HVC absorption that are similar to those derived in the TT sample. Therefore despite a non-uniformity in the S/N, the TT, GTO, and CSG09 samples can be merged and can be compared to the LH11 stellar sample. Fig. 4 shows that the detections are generally of high significance as otherwise weak absorption of Si III, Si II, C IV, C II would have been detected more frequently in the sample with better sensitivity. This implies that low total H column HVCs are not important and that the present sample is essentially complete.

3 COVERING FACTOR AND DISTANCE OF THE HVCs

The sky covering factor of HVCs is a crucial quantity, as it is required to statistically determine the distance of the UV absorption-line selected population of HVCs (LH11) and for estimating the total mass of the HVCs ($M \propto f_c d^2$, where f_c is covering factor). Following LH11, we define two classes of HVCs: the HVCs with $90 \leq |v_{\text{LSR}}| \lesssim 170 \text{ km s}^{-1}$ and the VHVCs with $|v_{\text{LSR}}| > 170 \text{ km s}^{-1}$. The reason for this sepa-

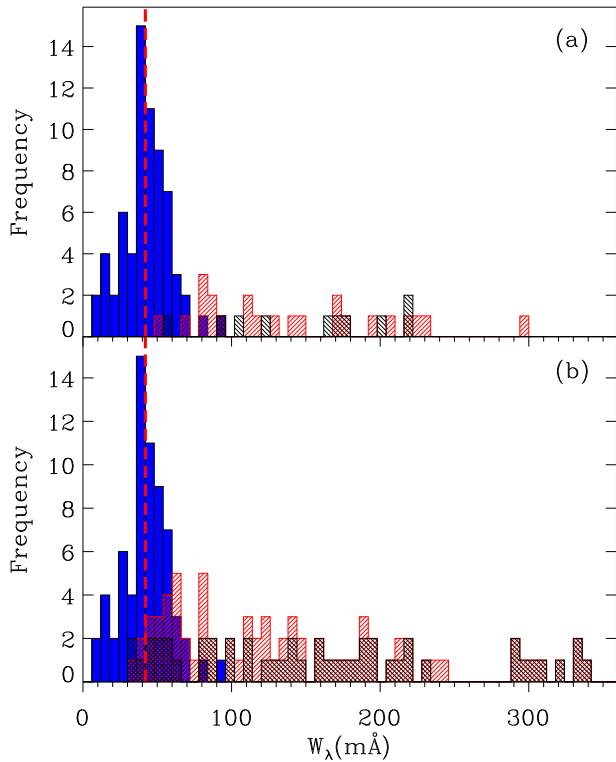


Figure 4. (a) Distribution of the HVC equivalent widths and equivalent width limits. The blue filled histogram represents the 3σ equivalent width detection limit of the AGN TT sample, with the vertical red dashed line being the median (42 mÅ) of this distribution. The red hashed histogram is the C II $\lambda 1334$ equivalent width of the HVC detected in the TT AGN sample. The black hashed histogram is the C II $\lambda 1334$ equivalent width of the HVC detected in the LH11 stellar sample. (b) Same as (a), but the red hashed histogram is the Si III $\lambda 1206$ equivalent width of the HVC detected in the CSG09 AGN sample and black hashed histogram shows the distribution of the strongest HVC component along each line of sight of the CSG09 AGN sample.

ration in velocity is that HVCs were detected toward stars, but no VHVC absorption was found in the stellar spectra; the precise velocity cutoff is somewhat arbitrary (as is the lower bound at 90 km s^{-1} , see §3.4 for more details). In Table 3, we summarize the values of f_c for different AGN samples and the LH11 stellar sample (see LH11 and §4). In this table, m is the sample size (i.e., the number of sightlines). We assess a 68% confidence interval for each value of f_c using the Wilson score interval for a binomial distribution. The main results can be visualized in Fig. 5, are listed in Table 3, and can be summarized as follows:

- (i) f_c does not strongly depend on the sensitivity of the present data;
- (ii) Comparing the H I surveys with ours, we conclude that 74% of the HVC+VHVC directions have $N(\text{H I}) < 3 \times 10^{18} \text{ cm}^{-2}$ and 46% have $N(\text{H I}) < 8 \times 10^{17} \text{ cm}^{-2}$ (panel (a) in Fig. 5);
- (iii) the HVC detection rates in the stellar and AGN samples overlap within 1σ , strengthening the LH11 conclusion that most of the HVCs are near the Milky Way disk, within about heliocentric distances 5–15 kpc (panel (b) in Fig. 5);

Table 3. Covering factors for the HVCs and VHVCs

	m	$f_c(\text{HVC})$ (%)	$f_c(\text{VHVC})$ (%)	$f_c(\text{HVC} + \text{VHVC})$ (%)
TT AGN Sample with $W_{\text{lim}} \geq 10 \text{ mÅ}$				
all b	67	58 ± 6	6_{-2}^{+4}	63 ± 6
$b > 0^\circ$	60	58 ± 6	3_{-2}^{+3}	62 ± 6
TT AGN Sample with $10 \leq W_{\text{lim}} \leq 42 \text{ mÅ}$				
All b	34	59 ± 9	6_{-3}^{+5}	62 ± 9
$b > 0^\circ$	31	58 ± 9	7_{-3}^{+6}	61 ± 9
TT+GTO+CSG09 AGN sample				
all b	133	59 ± 4	20 ± 4	64 ± 4
$b > 0^\circ$	105	57 ± 5	13 ± 3	61 ± 4
$b < 0^\circ$	28	68 ± 9	46 ± 10	75_{-9}^{+7}
LH11 stellar sample				
all b , $d > 3 \text{ kpc}$	28	50 ± 9	0_{-0}^{+3}	50 ± 9
all b , $d > 5 \text{ kpc}$	20	60 ± 10	0_{-0}^{+5}	60 ± 10

Note: m is the size of the considered sample. Errors are 68.3% level confidence interval estimated from the Wilson score.

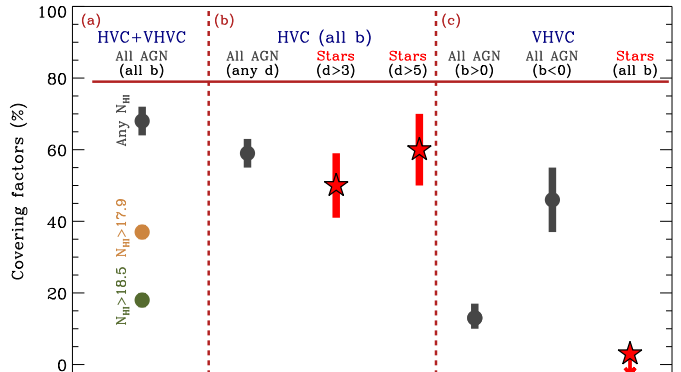


Figure 5. Covering factors for the HVCs and VHVCs: (a) comparison between the H I emission ($N(\text{H I})$ limited) and UV absorption (any $N(\text{H I})$, i.e., $N(\text{H I}) \lesssim 10^{15} \text{ cm}^{-2}$ to $N(\text{H I}) \gtrsim 10^{20} \text{ cm}^{-2}$) samples; (b) comparison the covering factors determined from the TT+GTO+CSG09 AGN and LH11 stellar (where two different heliocentric distances cutoff are considered at 3 and 5 kpc) samples; (c) VHVC covering factor from the TT+GTO+CSG09 AGN and LH11 stellar samples.

(iv) the HVC detection rate in the stellar sample drops with decreasing distances (panel (b) in Fig. 5);

(v) VHVCs are far more frequent at $b < 0^\circ$ than at $b > 0^\circ$, which is largely due to large Galactic sky covering of the Magellanic Stream at $b < 0^\circ$ (panel (c) in Fig. 5).

In the following sections, we explain and discuss these conclusions.

3.1 HVC covering factor from the AGN samples

We first consider solely the TT sample because we are certain that no bias was introduced in selecting the targets that would favor or disfavor the detection of HVCs. In order to

confirm that our HVC samples are essentially complete, we consider one sample with $W_{\text{lim}} \geq 10$ mÅ (i.e., the entire TT sample) and a sample with $10 \leq W_{\text{lim}} \leq 42$ mÅ (i.e., a sample with a higher sensitivity). The results are summarized in Table 3. The entire and more sensitive TT samples show that f_c is essentially independent of the equivalent width sensitivity of the present data (a sample with $W_{\text{lim}} \geq 42$ mÅ gives $f_c = 56\%$, similar to the f_c -values listed in Table 3). As demonstrated in Fig. 4 and discussed in §2.4, there is no evidence for a large population of weak metal absorbers with a significant f_c .

Fig. 1 shows that there is no HVC at $b > 75^\circ$ in the TT sample, which is also confirmed with the combined sample (see Fig. 6). For $30^\circ < b < 75^\circ$ the HVC detection rate is necessarily higher at 69% compared with 58% for the $b > 0^\circ$ sky. The absence of HVCs at $b > 75^\circ$ could be due in part to statistical fluctuations over the small solid angle covered by these latitudes. If the HVCs follow a thickened disk-like distribution, a deficit of clouds at $b > 75^\circ$ would also be more likely.

In Fig. 6, we show the distribution of sightlines and HVC detections for the combined sample that includes the TT, GTO, and CSG09 samples. This combined sample has much better coverage at $b < 0^\circ$ where it is larger than the TT sample by a factor 4. The observations are still heavily weighted toward the northern Galactic sky. In Table 3, we summarize the detection rates of the combined sample. We again consider the HVC, VHVC, and HVC+VHVC categories in 3 sub-samples: the entire Galactic sky, the northern Galactic hemisphere ($b > 0^\circ$), and the southern Galactic hemisphere ($b < 0^\circ$).

For $b > 0^\circ$, the hit rates are very similar for the HVC and HVC+VHVC between the TT and full samples. Within the errors the VHVC hit rate is also similar and small at $b > 0^\circ$. Comparing the entire sky yields similar conclusions, but again the sample is heavily weighted to $b > 0^\circ$ with ~ 4 times more AGN than at $b < 0^\circ$. Given this similarity, we will adopt the results from the combined sample for the remainder of this work. There is, however, a clear difference at $b < 0^\circ$: the covering factor of the VHVC is substantially larger, with a 46% covering factor compared to 13% at $b > 0^\circ$ (see Table 3 and Fig. 5). There is also a tentative increase in $f_c(\text{HVC})$ at $b < 0^\circ$ compared to that at $b > 0^\circ$, although the values overlap with the errors. As we discuss further in §3.4, the southern Galactic sky is dominated by the Magellanic Stream (Putman et al. 1998; Nidever et al. 2008), and this mostly explains the considerable difference in $f_c(\text{VHVC})$ between the two Galactic hemispheres. We defer a discussion on the sky coverage of the VHVCs and implications for the origins and distances of the VHVCs to §3.4.

The covering factors derived from our samples using O I, C II, C IV, Si II, Si III, Si IV etc., are quite consistent with those determined for HVCs with O VI absorption, which are in the range of 60%–75% (Sembach et al. 2003; Fox et al. 2006). The fact that the covering factors are similar is not surprising in view of the multiphase nature of the HVCs, which often show absorption by O I, C II, C III, C IV, O VI at similar velocities in a given sightline (e.g., Ganguly et al. 2005; Collins et al. 2005; Fox et al. 2004, 2006; Zech et al. 2008). As warm HVCs move in the Galactic halo, some of the “O VI HVCs” are likely the collisionally ionized inter-

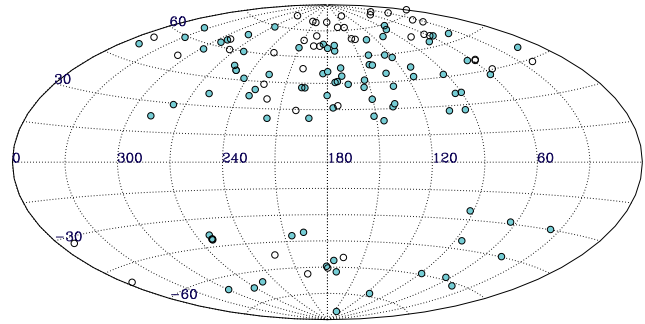


Figure 6. Aitoff projection of the combined (TT+GTO+CSG09) sample. A filled circle means at least one HVC with $|v_{\text{LSR}}| > 90$ km s $^{-1}$ is detected along the line of sight. An open circle means that no HVC is detected along the sightline.

face between the hot Galactic corona and the cooler ionized and neutral HVCs (e.g., Sembach et al. 2003; Collins et al. 2005; Kwak et al. 2011).

We note that the difference in the hit rates between our analysis and CSG09 (and Shull et al. 2009, where they found $f_c(\text{HVC} + \text{VHVC}) = 80\text{--}90\%$ based on the search of Si III HVC absorption in AGN spectra) is due to three causes: i) there was a bias in the CSG09 sample where AGN initially targeted for HVC science were not removed, which artificially increased the covering factor; ii) while CGS09 confirmed in many cases the HVC absorption with ions other than Si III, in several cases they rely solely on the Si III absorption and *assumed* that the intergalactic contamination is small; and iii) as we have just demonstrated, the TT and combined samples are not uniformly distributed in both hemispheres, thus our sample weights the northern hemisphere more strongly than CSG09 (and the CSG09 sample is more balanced between the two Galactic hemispheres). A uniform measure of the entire Galactic sky covering factor of the HVC+VHVC would likely be somewhat higher than the 64% derived here. In view of this imbalance, a straight average between the two Galactic hemispheres is more appropriate, yielding a covering factor for the entire sky of $f_c(\text{HVC} + \text{VHVC}) = 68\% \pm 4\%$. That is the value adopted in Fig. 5 (panel (a)).

3.2 Distance of the HVC population

Having set a robust HVC covering factor of $f_c(\text{HVC}) = 59\% \pm 4\%$ toward the AGN sightlines, we can revisit the LH11 method to statistically determine the distance of the HVC population by comparing the HVC covering factors determined toward sightlines with no distance limits (AGN) and with distance limits (stars). With their stellar sample, LH11 found $f_c(\text{HVC}) = 50\% \pm 9\%$ ($m = 28$). The f_c -values of the AGN and LH11 stellar samples are therefore consistent within the 68% confidence interval (see also Table 3 and Fig. 5). The same ions and techniques were used to search for the HVC absorption in the stellar and AGN spectra, although finding HVC absorption in the stellar sample often relied only on C II and Si II (Si III was often too noisy and C IV could be blended with the stellar absorption). While it may be possible for more highly ionized HVCs to be missed in the stellar sample, this is unlikely to be important since

a large majority of the HVCs would still show absorption in C II and Si II as discussed in §2.3.

Although the results are consistent within a 68% confidence interval, the difference between the stellar and AGN f_c values is large enough that it could suggest a fraction of HVCs being at much greater distances if f_c is not distance-dependent. However, owing to interstellar drag on these clouds, HVCs should slow down as they fall onto the Milky Way disk (Benjamin & Danly 1997). More recent hydrodynamical simulations have also followed the infall of HVCs through the Galaxy and predict that the HVCs become disrupted by their interaction with the corona (e.g., Bland-Hawthorn et al. 2007; Peek et al. 2008; Heitsch & Putman 2009; Kwak et al. 2011; Joung et al. 2012). These two arguments imply that the number of HVCs should decrease at smaller d or z . As LH11 selected their stellar sample so that the stars are at $|z| \gtrsim 3$ and $d > 3$ kpc (only one star was at $z = -2.6$ kpc, but $d = 8.7$ kpc), we searched MAST for stars at smaller distances $d > 2$ kpc (setting this limit to avoid probing only our local environment) and $|z| > 1$ kpc (and $|b| > 15^\circ$ to avoid probing HVCs linked to phenomena occurring in the Galactic disk, see, e.g., Lehner et al. 2011) to study the dependence between f_c and d . We found an additional 8 stars that satisfy these criteria with the appropriate coverage of at least C II $\lambda 1334$, Si II $\lambda 1260$, Si III $\lambda 1206$. We summarized the full (LH11 plus 8 stars) stellar sample in Table 4, where the stars are ordered in z -height from the Galactic plane.

With this sample of stars, we estimate the values of f_c as function of d or $|z|$, i.e., we calculated f_c for stars with $d > 2$ kpc (at any $|z| > 1$ kpc), > 3 kpc, etc., and similarly with $|z|$ (and any $d > 2$ kpc). The results are summarized in Fig. 7 where there is a distinct trend between f_c and d, z . At $d \lesssim 3$ –4 kpc ($|z| \lesssim 2$ –3 kpc), f_c is smaller and not consistent within the 68% confidence interval with f_c determined from the AGN sample, but as d ($|z|$) increases, f_c increases, and plateaus at $d > 4$ kpc ($|z| > 3$ kpc) to the f_c value determined from the AGN sample. For $d \gtrsim 5$ kpc ($|z| > 3$ –4 kpc), $f_c = 61\% \pm 10\%$, in remarkable agreement with the result from the AGN sample. Based on this result, if we set a cutoff at $z = 4$ kpc, we find:

- $|z| \geq 4$ kpc, $f_c = 58\% \pm 11\%$ ($\langle d \rangle = 11.5 \pm 6.5$ kpc);
- $|z| < 4$ kpc, $f_c = 20\%^{+12\%}_{-8\%}$ ($\langle d \rangle = 4.1 \pm 1.8$ kpc).

A larger sample of stars would be needed to better characterize the infall of HVCs onto the Galactic disk, but our results strongly suggest that the population of HVCs decreases with decreasing $|z|$ (and d), and hence the HVCs may either be disrupted or decelerated to become intermediate-velocity clouds (IVCs, $50 \leq v_{\text{LSR}} < 90$ km s $^{-1}$) or low-velocity clouds. A detail description of the (UV-selected) IVC population is beyond the scope of this work, but it would be extremely valuable to undertake to understand how HVCs may reach the Galactic disk.

The excellent agreement in the HVC detection rates between the stellar and AGN samples strengthens the conclusions reached by LH11: most of the HVCs are within 5–15 kpc of the sun. The drop in the population of HVCs with $|z|$ is consistent with models predicting their fall through the Galactic halo onto the disk. All this implies that the HVCs are distant enough to have sufficient mass and close enough

Table 4. Stellar sample with stars at $d > 2$ kpc, $|z| \geq 1$ kpc

Name	l ($^\circ$)	b ($^\circ$)	d (kpc)	$ z $ (kpc)	$v_{\text{LSR}}^{\text{HVC}}$ (km s $^{-1}$)
HD195455 ^a	61	−27	2.2	1.0	+94
HD116852 ^a	304	−16	4.5	1.3	...
HD215733 ^a	85	−36	2.9	1.7	... ^b
HD149881 ^a	31	+36	2.9	1.7	...
JL212 ^a	303	−61	2.2	1.9	...
NGC6723-III60	0	−17	8.7	2.6	−90
HD100340 ^a	258	61	3.0	2.6	...
HD18100 ^a	217	−62	3.1	2.7	...
HD119608 ^a	320	43	4.1	2.8	...
HD121968	334	+55	3.8	3.1	...
PG1511+367	59	+59	3.8	3.2	...
NGC104-UIT14	306	−45	4.5	3.2	...
HD233622	168	+44	4.7	3.3	...
EC10500-1358	264	+40	5.2	3.3	+97
PG1704+222	43	+32	6.9	3.6	...
PG0855+294	196	+39	6.5	4.1	+93, +107
PG2219+094	73	−40	6.6	4.2	...
PG0832+675	148	+35	7.5	4.3	−123
PG0955+291	200	+52	5.5	4.3	...
NGC6341-326	68	+35	8.2	4.7	−94 :
NGC6205-Barnard29	59	+41	7.7	5.0	−107
NGC5904-ZNG1	4	+47	7.2	5.3	−140, −120
PG1610+239	41	+45	8.4	5.9	...
HS1914+7139	103	+24	14.9	6.0	−175, −118
PG0122+214	133	−41	9.6	6.2	−160, −91
PHL346	41	−58	8.7	7.4	...
SB357	301	−81	7.9	7.8	...
PG0914+001	232	+32	16.0	8.4	+100, +170
PG0009+036	105	−58	10.8	9.1	...
vZ 1128	43	+79	10.2	10.0	...
PG1708+142	35	+29	21.0	10.0	...
PG1002+506	165	+51	13.9	10.8	−102, +101
NGC5824-ZNG1	333	+22	32.0	12.0	−160 :
PG1323-086	317	+53	15.8	12.6	−91

Note: *a*: Stars not originally in the LH11 stellar sample. *b*: There is an IVC at $v_{\text{LSR}} = -84$ km s $^{-1}$ Fitzpatrick & Spitzer 1997. A colon means the result is tentative in view of the low signal-to-noise of the data (removing these stars from the sample would not change our conclusions).

that their infall rate balances the star formation rate in the disk of the Milky Way (see LH11 and §5.2). In §4 we also show that several of the ionized HVCs are closely related to the large H I complexes given their proximity on the celestial sphere and in three dimensional space. The (neutral and ionized) HVCs are therefore very likely a large part (if not all) of the source of gas required for continued star formation.

3.3 HVC covering factors from H I emission and UV absorption data

Searching for high-velocity H I emission with $|v_{\text{LSR}}| \geq 90$ km s $^{-1}$ using the LAB survey toward the sightlines in the combined sample, we find $f_c \simeq 18\%$ for $\log N(\text{H I}) \gtrsim 18.5$. Given that more sightlines in the CSG09 and GTO samples go through large H I HVC complexes (Magellanic Stream, complex C and complex A), it is not surprising that the H I LAB HVC detection is higher in these samples ($f_c \sim 22\%$) than in the TT sample ($f_c \sim 12\%$). The detection rate from

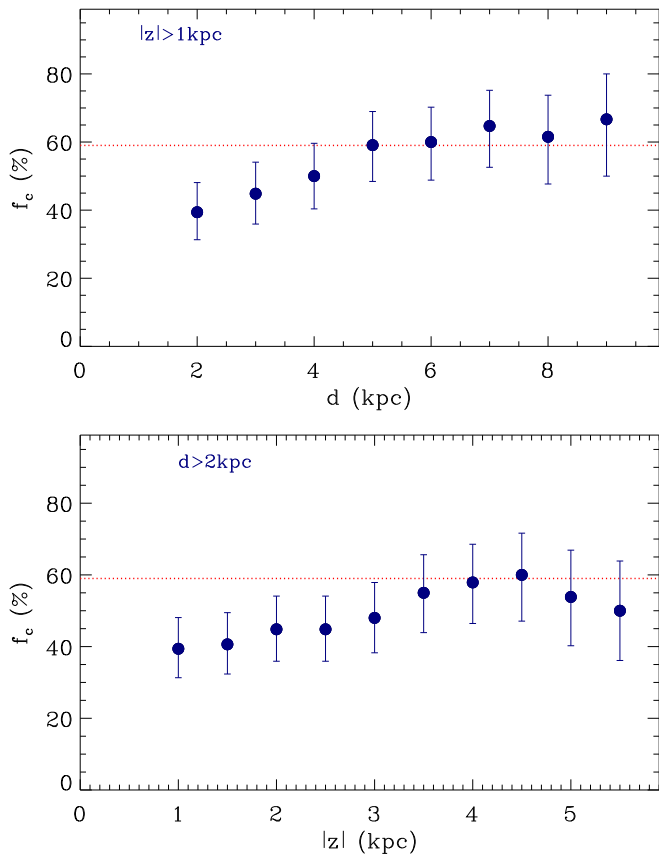


Figure 7. The HVC covering factors toward the stars in the stellar sample summarized in Table 4, which includes the LH11 stellar sample plus 8 stars at $1 < |z| < 3$ kpc. *Top panel:* f_c vs. d . Each data point corresponds to the value of f_c for stars at distances $> d_i$, where $d_i = 2, 3, \dots$ kpc. The horizontal dotted line is the HVC covering factor determined toward the AGN. *Bottom panel:* same as top panel but f_c is shown against z . As stars with smaller d or $|z|$ are removed from the sample, f_c converges on the f_c -value determined from the AGN sample.

the combined sample is entirely consistent with that derived for the entire radio H I sky survey at a similar sensitivity (Wakker 1991). We emphasize this result as the techniques are different and the absorption-line method samples comparatively sparsely the Galactic sky. Our AGN sample and the absorption-line technique are well suited for finding HVCs with both high and low H I column densities.

Deeper radio H I emission surveys reached a sensitivity of $\log N(\text{H I}) \simeq 17.9$ (Murphy et al. 1995; Lockman et al. 2002). At this limit, 37% of the sky is covered by H I HVCs+VHVCs, which is still substantially smaller than f_c in our UV absorption survey. Extrapolating to $\log N(\text{H I}) \simeq 17$, Lockman et al. (2002) argued that the HVC+VHVC covering factor would be about 60%, close to our findings ($f_c = 68\%$). However, they assume that the constant covering factor per decade of $\log N(\text{H I})$ observed between 19 and 17.9 dex applies down to 17 dex. While direct estimates of $N(\text{H I})$ via H I absorption is difficult, Fox et al. (2006) searched for H I Lyman series absorption associated with O VI and/or C III HVCs. Their results show that the H I column densities vary tremendously: the low-

est column UV-selected HVCs have $\log N(\text{H I}) \lesssim 14.7\text{--}15.0$ while the highest have $\log N(\text{H I}) \gtrsim 20$; thus there is at least a 5 dex range in $N(\text{H I})$. The detection of O VI or C III or any other metal line species in low H I column density HVCs still implies $N(\text{H}) > 10^{17}\text{--}10^{18}(Z/Z_\odot)^{-1} \text{ cm}^{-2}$. Thus, even though the H I column density in these HVCs may be small, the total hydrogen column densities can still be substantial.

Comparing the H I surveys with ours, the relative covering factors imply about 74% of the HVC+VHVC directions have $N(\text{H I}) < 3 \times 10^{18} \text{ cm}^{-2}$ and 46% have $N(\text{H I}) < 8 \times 10^{17} \text{ cm}^{-2}$. We emphasize again the population of HVCs with extremely low total H column density is unimportant (see §2.4).

3.4 Covering factor and distribution of the VHVCs

LH11 did not find any HVCs with $|v_{\text{LSR}}| \gtrsim 170 \text{ km s}^{-1}$, the so-called VHVCs, in absorption in the stellar spectra. They concluded that the VHVCs must be at distances $d > 10\text{--}20$ kpc. Our analysis of the covering factors of VHVCs using the much larger sample of AGN demonstrates that at $b > 0^\circ$, the covering factor is quite small, $f_c(\text{VHVC}) \simeq 13\%$ (see Table 3 and Fig. 5). In fact the TT sample nearly completely missed the VHVCs. The LH11 stellar sample and TT AGN sample are distributed similarly across the Galactic sky (see Fig. 1), but the LH11 sample is about 2.5 times smaller. It may not be therefore surprising that no VHVC absorption was observed in the spectrum of a star ($f_c(\text{VHVC}) \lesssim 13\%$ for a 95% confidence interval for the stellar sample). Some of the stars cover the $b < 0^\circ$ hemisphere where the $f_c(\text{VHVC})$ is much larger, but, as we show below, most of the VHVC absorption is associated with the Magellanic Stream. The absence of Magellanic Stream absorption toward stars confirms that the Stream is indeed far away. Using our large sample of AGN, we can learn more about the origins of these clouds as we now demonstrate.

In Fig. 8, we show the sky distribution of VHVC absorption from our combined sample as well as H I 21-cm emission from the NRAO 140-ft ($\log N(\text{H I}) \geq 17.9$) observations of Lockman et al. (2002). We do not show the lower velocity HVCs in order to highlight solely the VHVCs. In this figure, open symbols are used if no VHVC is seen in absorption or emission. In the bottom panel of this figure, the VHVCs with $|v_{\text{LSR}}| > 170 \text{ km s}^{-1}$ are shown, while the top shows only the VHVCs with $|v_{\text{LSR}}| > 210 \text{ km s}^{-1}$. The overall sky coverage is excellent with only a lack of H I data in the $b < 0^\circ$ and $240^\circ < l < 360^\circ$ quadrant because this region of the sky cannot be observed from Green Bank. The velocity distribution seen in emission and absorption is strikingly similar, which reinforces that the VHVCs seen in emission and absorption must be similar structures with different ionization levels (see §4). It is therefore not surprising that there is a remarkable correlation between these maps and all sky H I 21-cm HVC map (e.g., Wakker et al. 2003), with many of the VHVCs superimposed onto or near large known H I HVC complexes; the Magellanic Stream at similar velocities, complexes C and A, the anti-center HVCs at higher velocities. Wakker (2001) and Lockman et al. (2002) attributed the gas moving at velocities with $-210 \lesssim v_{\text{LSR}} \lesssim -170 \text{ km s}^{-1}$ in the $b > 0^\circ$ and $0^\circ < l < 180^\circ$ quadrant pri-

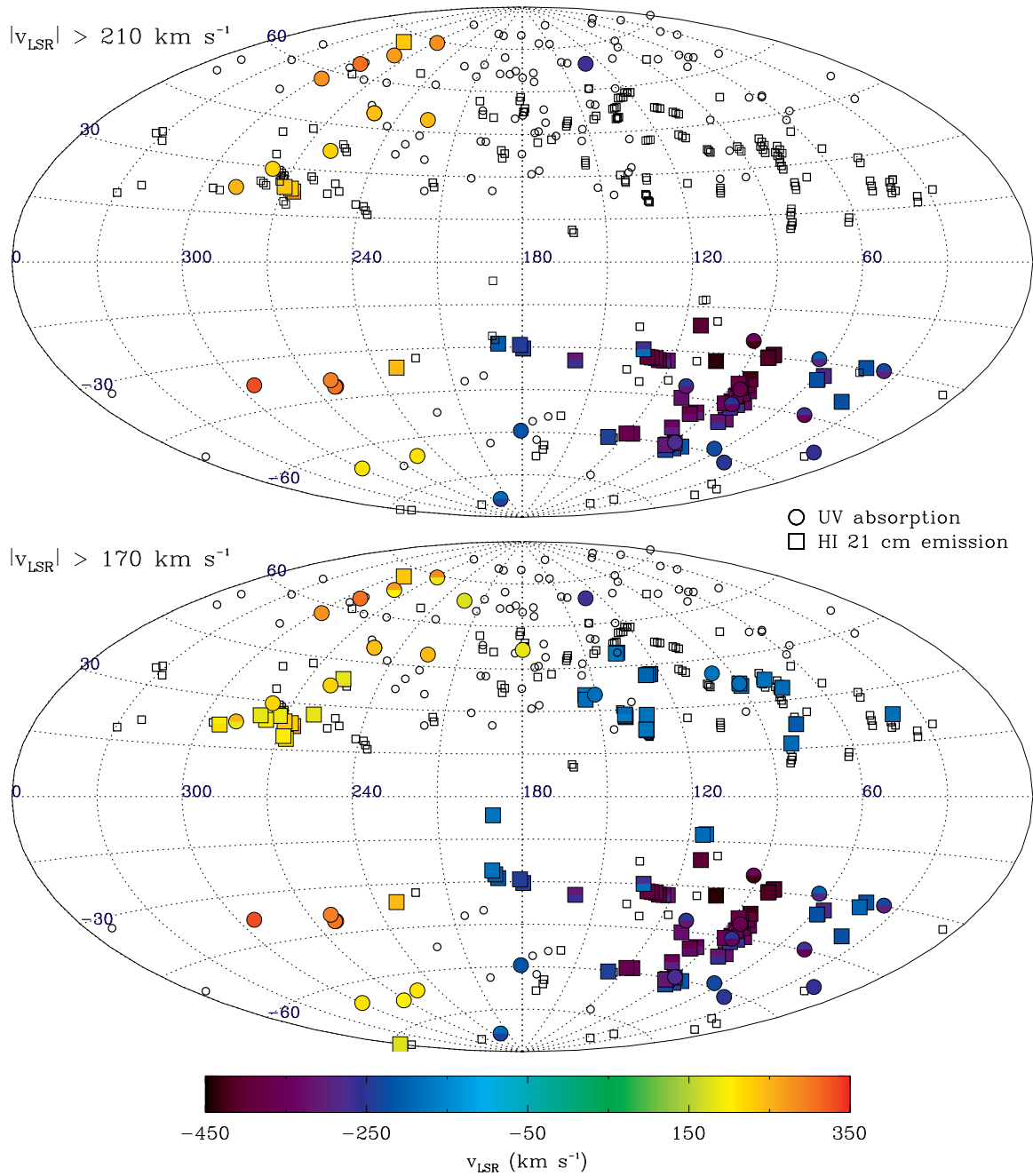


Figure 8. Aitoff projection maps showing the sightlines where a VHVC is detected toward an AGN (filled *circles* from UV absorption TT+GTO+CSG09 data; filled *squares* from the H I 21-cm emission data from Lockman et al. 2002). On the *top* panel, detections are VHVCs with $|v_{\text{LSR}}| > 210 \text{ km s}^{-1}$, while on the *bottom* panel, detections are VHVCs with $|v_{\text{LSR}}| > 170 \text{ km s}^{-1}$. The region defined by $b < 0^\circ$ and $240^\circ < b < 360^\circ$ cannot be observed from Green Bank, explaining the lack of H I emission data in this region. All the open symbols indicate that no VHVC absorption or emission with $|v_{\text{LSR}}| > 210 \text{ km s}^{-1}$ (*top*) or $|v_{\text{LSR}}| > 170 \text{ km s}^{-1}$ (*bottom*) is found along the sightline.

marily to complex C. In the top panel of Fig. 8, where we only show now the VHVCs with $|v_{\text{LSR}}| > 210 \text{ km s}^{-1}$, the VHVCs affiliated with complex C have almost completely disappeared (as well as some of the anti-center complex). The VHVCs that remain present correlate extremely well with the H I map of the Magellanic stream and its leading arm (Wakker et al. 2003; Nidever et al. 2008), except

that the most sensitive H I emission and UV absorption data suggest it could be wider (i.e., the Stream has a large ionized envelope) and could reach higher positive galactic latitudes than previously thought. Some of the VHVCs near $l = 120^\circ-130^\circ$ and $b = -20^\circ$ to -30° are likely associated with the M31 and M33 galaxies (Thilker et al. 2004; Westmeier et al. 2005; Putman et al. 2009), but their solid angle

Table 5. Heliocentric distance (d_{HVC}), height ($|z_{\text{HVC}}| = d_{\text{HVC}}|\sin b|$), and Galactocentric distance^a (R_G) of the HVCs and association with H I HVC complex

Name	l (°)	b (°)	d_{HVC} (kpc)	$ z_{\text{HVC}} $ (kpc)	R_G (kpc)	$v_{\text{LSR}}^{\text{HVC}}$ (km s ⁻¹)	Associated H I HVC Complex	Stellar Distance References
NGC6723-III60	0	-17	< 8.7	< 2.6	< 0.2	-90	None	(1)
NGC5904-ZNG1	4	+47	< 7.5	< 5.5	< 3.4	-140	Complex L?	(1)
NGC5904-ZNG1	4	+47	< 7.5	< 5.5	< 3.4	-120	Complex L?	(1)
M13-Barnard29	59	+41	< 7.1	< 4.7	< 7.4	-121	Complex C	(1)
HD195455 ^b	61	-27	< 2.2	< 1.0	< 7.7	+94	Complex gp?	(2)
HS1914+7139	103	+24	< 14.9	< 6.0	< 17.6	-118	Outer Arm/Complex C?	(3)
HS1914+7139	103	+24	< 14.9	< 6.0	< 17.6	-175	Complex C	(3)
PG0122+214	133	-41	< 9.6	< 6.2	< 14.5	-91	Cohen Stream	(3)
PG0122+214	133	-41	< 9.6	< 6.2	< 14.5	-160	WW503	(3)
PG0832+675	148	+35	≥ 8.1	≥ 4.7	≥ 14.6	-145	Complex A	(4)
PG0832+675	148	+35	< 8.1	< 4.7	< 14.6	-123	Ionized complex A?	(4)
PG1002+506	165	+51	< 13.9	< 10.8	< 17.1	-102	Complex M	(5)
PG1002+506	165	+51	< 13.9	< 10.8	< 17.1	+101	None	(5)
PG0855+294	196	+39	< 6.5	< 4.1	< 13.4	+93	Cloud WW113	(6)
PG0855+294	196	+39	< 6.5	< 4.1	< 13.4	+107	Cloud WW113	(6)
PG0914+001	232	+32	< 16.0	< 8.4	< 20.0	+100	Complex WB	(6)
PG0914+001	232	+32	< 16.0	< 8.4	< 20.0	+170	Complex WA	(6)
EC10500-1358	264	+40	< 5.2	< 3.3	< 9.8	+97	Cloud WW95	(2)
NGC104-UIT14	306	-45	> 4.5	> 3.2	> 7.1	... ^c	Complex WE	(1)
PG1323-086	317	+53	< 15.8	< 12.6	< 6.7	-91	None	(7)

(a): Galactocentric distance of the HVCs, where $R_G = (R_\odot^2 + (d_{\text{HVC}} \cos b)^2 - 2d_{\text{HVC}} R_\odot \cos l \cos b)^{0.5}$, assuming the distance from the Sun to the Galactic center $R_\odot = 8.5$ kpc. (b): Not in the LH11 sample. (c): No absorption is detected, but strong H I emission is observed along this line of sight. References for the heliocentric distances of stars that were used to estimate the distance limits of the HVCs: (1) Harris 1996, 2010; (2) Rolleston et al. 1997; (3) Ramspeck et al. 2001, (4) Wakker 2001, (5) Ringwald et al. 1998, (6) Rolleston et al. 1999, (7) Moehler & Heber 1998.

is extremely small. We therefore conclude that most of the VHVCs with $|v_{\text{LSR}}| > 210$ km s⁻¹ are dominated by the Magellanic Stream at $b < 0^\circ$ and its leading arm at $b > 0^\circ$. Only a very few of the VHVCs, such as those associated with M31 and M33, may not be part of the Stream. Independently, Putman et al. (2011) showed recently that many compact VHVCs have a head-tail structure (a signature of interaction with a hot diffuse medium) and can be associated with the Magellanic Stream. From our discussion, these small head-tail H I VHVCs must have larger envelopes of photoionized gas and collisionally ionized gas. The VHVCs are therefore not randomly distributed on the Galactic sky and appear mostly to be associated to known large structures. However, while our AGN sample is large, the Galactic sky can only be probed sparsely along pencil-beam sightlines with the absorption technique. It is therefore quite plausible that we might miss a population of compact HVCs with very small angular scales at very large distances (or that they may be confused with the more nearby VHVCs) as those possibly found with the ALFALFA survey (Giovannelli et al. 2010). The compact HVCs are therefore the only remaining candidates for dark matter mini-halos in the HVC population.

4 ASSOCIATION OF THE NEUTRAL AND IONIZED HVCs IN 3D SPACE

Determining the distance of the HVCs has been critical for associating HVCs with flows occurring near the Milky Way rather than in the IGM of the Local Group and for quanti-

fying their basic physical properties. The distances to many H I HVCs have been determined using stars in direction of the H I contours with $N(\text{H I}) \geq 3 \times 10^{18}$ cm⁻². The high-velocity gas seen in absorption toward AGN outside the H I contours has previously been associated with the extended HVCs seen in 21-cm emission based on their angular proximity and similarity in velocities (e.g., Fox et al. 2004; Collins et al. 2005). With the LH11 stellar sample, we can go a step further and directly compare the distances of H I HVCs and HVCs seen in UV absorption. We emphasize that for most of the LH11 stellar sightlines, no H I 21-cm emission (at the LAB survey sensitivity) is observed.

To search for H I HVCs associated with the UV-selected HVCs, we used the H I maps in Wakker et al. (2003) and Wakker (2001) as well as information provided by B.P. Wakker (private communication, 2011). In Appendix A, we summarize in detail the relation between the HVCs seen in UV absorption for each sightline with the H I complexes, while in Table 5, we summarize the HVC distance constraints from the LH11 stellar sample for which the detection is unambiguously a high-velocity interstellar feature and the S/N was high enough for their reliable detection.² In this table, we also added the additional star at smaller

² Specifically the following 4 stars were not considered: NGC6341-326 and NGC5824-ZNG1 owing to the low S/N in their COS spectra, and PG1243+275 and PG0934+145 for stellar contamination as noted by LH11. For the latter star, there is a possibility that both stellar and interstellar high-velocity components are present at the same velocity.

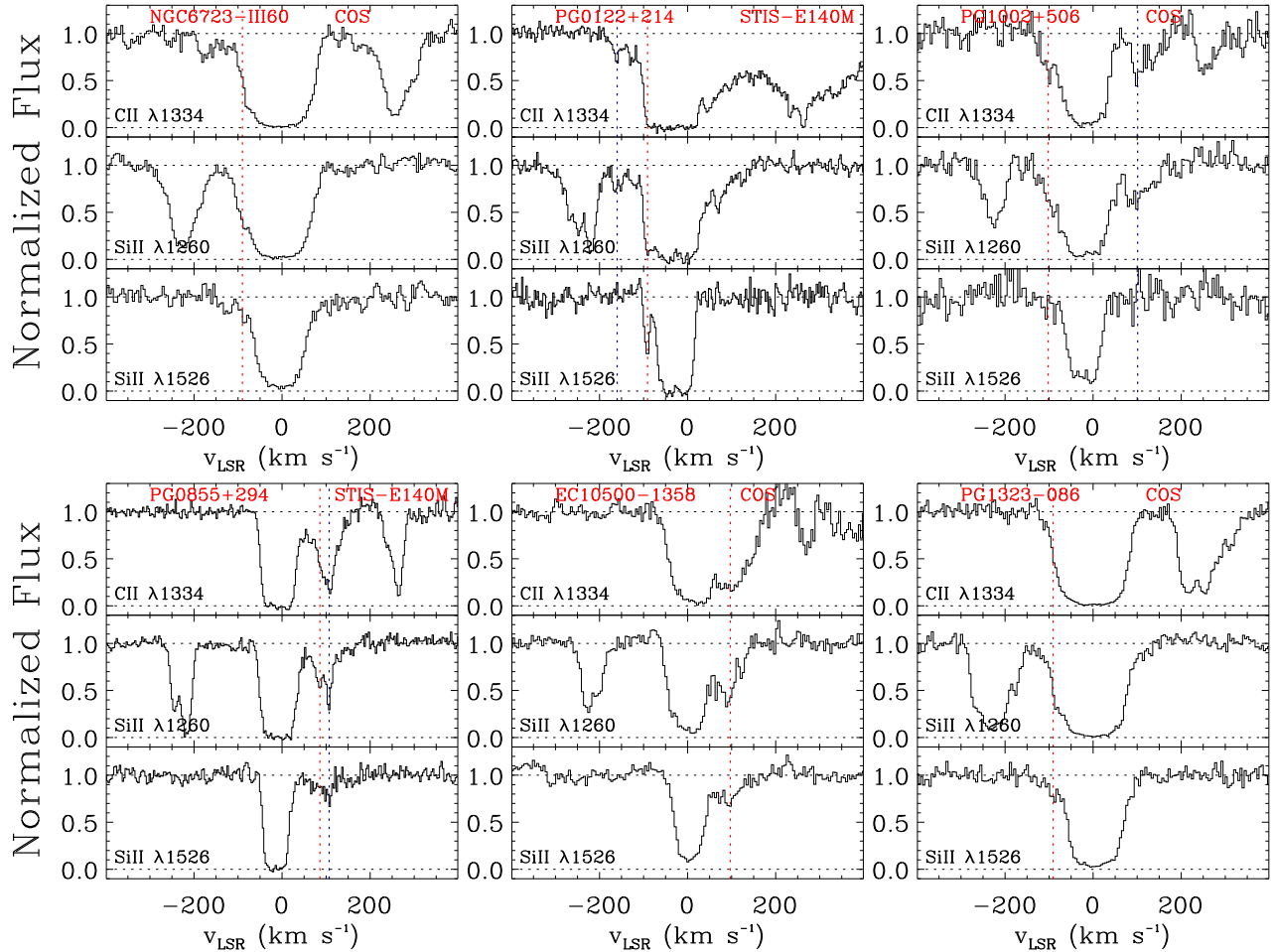


Figure 9. Normalized profiles of interstellar C II and Si II absorption seen in the spectra of several stars. The HVC components are marked by the vertical dotted lines. Other features are either stellar or interstellar. The spectra were normalized within $\pm 600 \text{ km s}^{-1}$ from the absorption lines using Legendre polynomials with a degree d_p (see, e.g., Lehner et al. 2011). For many stars, a fit with a low degree, $d_p = 1-3$, was used, but some stars (e.g., PG0855+294, EC10500-1358) have complicated stellar profiles, especially near C II, requiring higher values of $d_p > 6$. There is a broad stellar line next the interstellar C II feature at positive velocities in the spectrum of EC10500-1358 that is only approximately modeled (a feature that is similar to that seen in PG0122+214 that we did not attempt to remove in this case as no HVC is seen at positive velocities in this direction).

d with a HVC detection (see §3.2 and Table 4). The heliocentric distance, z -height above and below the Galactic disk, Galactocentric distance, velocity, and possible association with H I HVC complexes are listed in Table 5. We show the normalized interstellar absorption spectra in Figs. 9, 10, 11 for those stars whose STIS or COS spectra have not yet appeared in the literature (see Appendix A). We refer the reader to LH11 for more information about the data acquisition and reduction of the stellar sample. We emphasize that many of these HVCs are also detected in other transitions and/or species (e.g., O I, Al II, Si III, C IV, see figures in Lehner & Howk 2010, LH11, Zech et al. 2008, and Fig. 10).

From our detailed discussion in Appendix A and the results summarized in Table 5, we find that the distances to many of the predominantly ionized HVCs seen in the stellar spectra are consistent with the distances found for the H I HVCs nearby on the sky at similar LSR velocities. This implies that many of the HVCs seen in absorption are the extended diffuse envelopes of the denser clouds seen in

H I emission. In view of the much larger covering factor of the predominantly ionized HVCs and the proximity of the sightlines to many H I complexes, all the H I HVCs are likely to have extended ionized envelopes. However, in both the stellar and AGN sightlines there are also ionized HVCs where no H I complex is observed within 20° – 30° of the sightline, implying that the ionized high-velocity gas is not only found near H I complexes but also in regions devoid of H I 21-cm emission (at least for a H I sensitivity of about $> 3 \times 10^{18} \text{ cm}^{-2}$).

5 IMPLICATIONS

5.1 Origins of the gas flows in Milky Way halo

The results discussed in §3.2 and §4 have demonstrated that:

- (i) most of the HVCs are within about heliocentric distances 5–15 kpc,

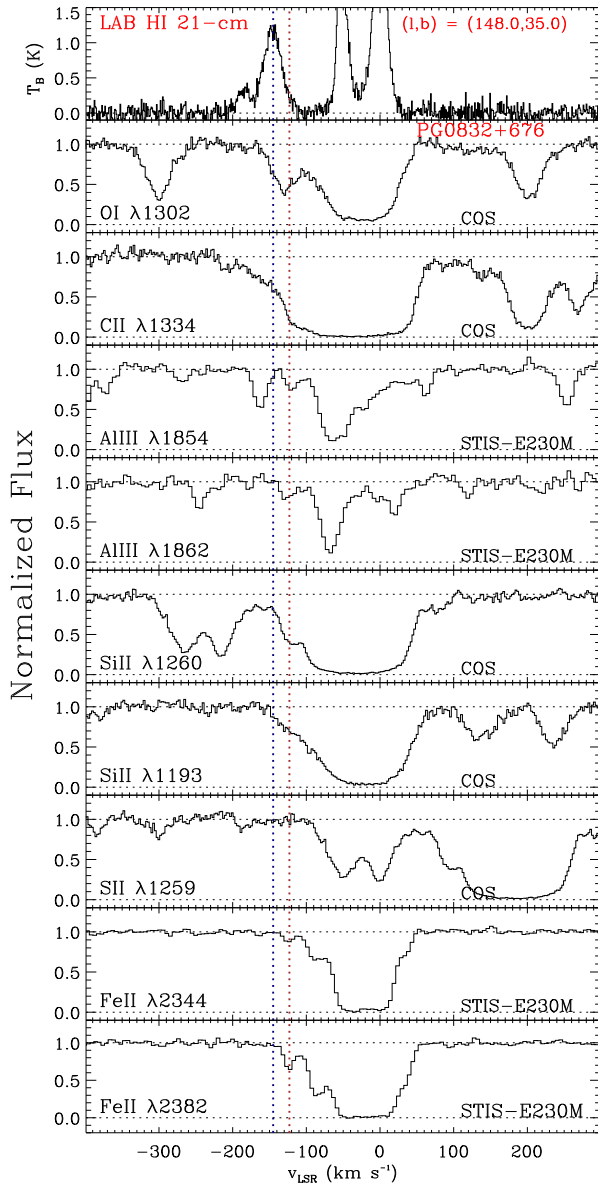


Figure 10. Normalized absorption profiles of various metal lines and LAB HI emission line profile (*top panel*) toward PG0832+675. The HVC components are marked by the vertical dotted lines. The main H I emission is observed at -145 km s^{-1} (note that the most negative emission component is not observed along this sightline using a $1'$ beam, Wakker et al. 2003) and is part of complex A. The main interstellar absorption is seen at -123 km s^{-1} , although some absorption is also seen at -145 km s^{-1} . The stellar spectrum is complicated with many stellar features (the stellar velocity is -70 km s^{-1} where absorption is seen in Al III as well as Si IV and C IV). We argue that PG0832+675 must be at the front edge of complex A and the -123 km s^{-1} component could be part of its ionized envelope.

(ii) the population of HVCs drops with decreasing distances or z -height, and

(iii) several HVCs seen in UV absorption are the extended ionized halos of their neutral counterparts.

The first item implies that HVCs represent flows occurring in the Milky Way halo within about one Galactic radius from

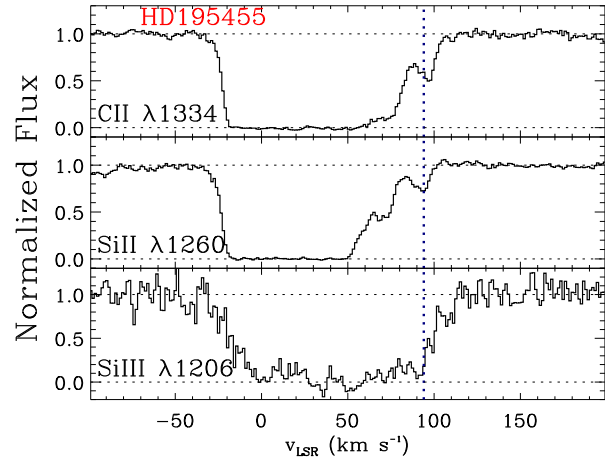


Figure 11. Normalized profiles of interstellar C II, Si II, Si III absorption seen in the STIS E140H spectrum of HD195455, which was not originally in the LH11 sample. The component at $+70 \text{ km s}^{-1}$ is consistent with the velocity of the IVC complex gp. The $+94 \text{ km s}^{-1}$ component might be a higher velocity component of this complex.

the Galactic center. The second item is consistent with in-fall of HVCs onto the Milky Way disk. With the third item, it is not a big leap to conclude that the metallicities UV-selected HVCs are similar to those of their H I counterparts. This is critical, as the metallicity can be difficult to estimate for the ionized HVCs, often requiring large ionization corrections (although see Zech et al. 2008). Past and current estimates of the metallicities of HVCs find a wide range of values from about a few percent solar to super-solar metallicity (e.g., Wakker 2001; Tripp et al. 2003; Collins et al. 2003; Fox et al. 2004; Zech et al. 2008; Shull et al. 2011; Yao et al. 2011; Tripp & Song 2012, B.P. Wakker, 2011, private communication), with a rough average around $0.2\text{--}0.4 Z_{\odot}$. As for their H I counterparts, several ionized HVC complexes must therefore have an extragalactic origin, i.e., not all are recycled gas recently ejected from the Milky Way (although we note that if some HVCs were ejected from regions situated at Galactocentric radii beyond $10\text{--}15 \text{ kpc}$, a metallicity of 0.4 solar would not be unjustified based on the Galactic abundance gradient, e.g., Chiappini et al. 2001).

While some of these HVCs may be the result of cold stream accretion wherein metal-poor gas flows onto galaxies along dense intergalactic filaments (Kereš & Hernquist 2009; Putman 2006) or remnants clouds from the Galaxy formation (Oort 1970; Peek et al. 2008), it is also possible that much of this gas may come from the interactions with nearby dwarf galaxies and their outflows. Such a scenario may be seen farther away with the Magellanic Stream and Large Magellanic Cloud outflows. The masses of the Stream and outflows from the LMC are quite substantial (Putman 2006; Nidever et al. 2008; Lehner et al. 2009). Being so far away, it is unclear if these HVCs will be able to reach the Galactic disk, instead they may mostly enrich the hot Galactic corona (Fox et al. 2010; Putman et al. 2011). However, it is not inconceivable to imagine that closer dwarf galaxies may feed the Milky Way disk via their outflows and tidally stripped material. One way to differentiate these scenarios would be to study the distribution of the HVC metallicities. At higher

redshifts H I absorbers with $16 \leq \log N(\text{H I}) \leq 18.5$ that trace the circumgalactic gas of galaxies (see §5.3) are sometimes observed at a metallicity of about 2% solar or less (Tripp et al. 2005; Ribaldo et al. 2011, N. Lehner et al. 2012, in preparation), and these may have originated from cold flow accretion (Ribaldo et al. 2011). HVCs with metallicity $< 2\%$ solar (like perhaps complex A, see Wakker 2001) could be candidates for cold stream accretion. On the other hand, for $> 20\%$ solar metallicity (like complex C), the gas has been polluted to levels as observed in the LMC outflows or Stream, which could be a signature of interaction between nearby dwarf galaxies and the Milky Way or of pollution of more metal poor gas by fountain or thick disk gas.

There are also HVCs with solar-like metallicity, suggestive of galactic fountain flows (e.g., Shapiro & Field 1976; Bregman 1980; Fraternali & Binney 2006). For example, Zech et al. (2008) derived a super-solar metallicity for two of these HVCs toward the Galactic center. This region is essentially devoid of H I emission at high-velocity (except for complex L), but high-velocity absorption is observed toward several AGN and stars (Sembach et al. 2003; Fox et al. 2006; Keeney et al. 2006; Zech et al. 2008; Bowen et al. 2008, this paper, see Appendix A). The high metallicity and absence of neutral gas are consistent with the HVCs tracing large-scale recycling flows within the central region of the Milky Way as those predicted by Galactic fountain models.

5.2 Fueling the Milky Way

As the HVCs with $90 \leq |v_{\text{LSR}}| \lesssim 200 \text{ km s}^{-1}$ are within a few kiloparsecs from the Milky Way irrespective of their H I content, they are also the most likely source of gas for fueling continued star formation in the Milky Way. Collins et al. (2005) and others argued that the segregation in positive and negative radial LSR velocity of HVCs with the Galactic coordinates (see Fig. 1) is consistent with an overall population of infalling clouds that reflect the sense of Galactic rotation, with some peculiar velocities. Although this is not a unique interpretation, our finding that the HVC population drops with decreasing z provides additional support to this conclusion as this drop is naturally explained if HVCs fall through the Milky Way halo onto the disk (see §3.2). A better characterization of the neutral and ionized HVC and IVC populations as a function of z will be needed to know if HVCs actually reach the Galactic disk, but our findings further support that they most likely feed the Galactic disk with new gas.

Because they both cover a large fraction of the sky and are at distances 5–15 kpc of sun, the HVCs with H I column density $\log N(\text{H I}) \lesssim 18.5$ represent a large mass reservoir. The total mass of the predominantly ionized HVCs is $M \approx 1.1 \times 10^8 (d/12 \text{ kpc})^2 (f_e/0.5) (Z/0.2Z_\odot)^{-1} M_\odot$, i.e., about $(0.2\text{--}2) \times 10^8 (Z/0.2Z_\odot)^{-1} M_\odot$ (see LH11). Even though the metallicity can vary from HVC to HVC (see above), this implies that the ionized gas mass is at least as important – and likely much more important than – the H I HVCs with $\log N(\text{H I}) \gtrsim 18.5$ (excluding the Magellanic Stream), which total about $10^7 M_\odot$ (Wakker 2001; Putman 2006; Wakker et al. 2007, 2008; Thom et al. 2008). The importance of the ionized HVCs to the total mass budget is also independently demonstrated by the deep H α emission

observations. The mass of ionized gas derived from these observations is similar to the H I mass within the H I contours (i.e., where $\log N(\text{H I}) > 18.5$), but the H α emission contours extend far beyond the H I contours (Hill et al. 2009; Barger et al. 2012), implying a greater mass of ionized gas.

While there is still some uncertainty in the fraction of the HVC population that is infalling, the metallicity, and the infall timescales, LH11 conservatively derived an infall rate of $0.4\text{--}1.4 M_\odot \text{ yr}^{-1}$. This is enough to balance the present-day total star formation rate ($1.9 \pm 0.4 M_\odot \text{ yr}^{-1}$) of the Milky Way (Chomiuk & Povich 2011) taken into account that the amount of infall needed to sustain star formation may be smaller than the star formation rate according to chemical evolution models (Chiappini et al. 2001) and stellar mass loss models (Leitner & Kravtsov 2011).

5.3 HVCs in the Local Group and beyond

Most of the HVCs identified so far in the Local Group are found near galaxies. In the Milky Way direct and indirect distance constraints place most of the HVCs and VHVCs within about 5–15 kpc (this paper, LH11 Wakker 2001; Putman et al. 2003), with only the Magellanic Stream possibly being much farther (Besla et al. 2012). Around M31 and M33, the H I HVCs are found within about 50 kpc, and many are within 15 kpc (Thilker et al. 2004; Westmeier et al. 2005, 2008; Putman et al. 2009). Deep H I observations have also revealed a tenuous filament of gas between M31 and M33 separated by about 150 kpc, which could be the result from a tidal interaction between these two galaxies (Braun & Thilker 2004). The HVCs observed toward the LMC probe outflows from the LMC and are also likely near the host galaxy (Lehner et al. 2009). HVCs in the Local Group of galaxies, including our Milky Way, are thus all within 10–50 kpc. While previously it could be argued that purely ionized HVCs could be farther away (e.g., Westmeier et al. 2008), our findings show that the ionized and neutral gas in HVCs are at similar distances, at least in the Milky Way halo. Although the sample of galaxies is small, there is therefore no evidence in our local galactic neighbor that ionized or neutral HVCs are found much beyond 1–2 galactic radii, except possibly for the remnants of galaxy interactions.³

If we move out from our local neighborhood, attempts have been made to connect QSO absorbers – in particular the optically thick absorbers (a.k.a., the Lyman limit systems, LLSs) – with the HVCs (e.g., Charlton et al. 2000; Richter et al. 2009). While some of the LLSs are likely higher redshift analogs of HVCs, we emphasize that the distances of HVCs place them close to galaxies. HVCs also probe “absorbers” with virtually any $N(\text{H I})$ and therefore likely include the population of both weak and strong Mg II absorbers.

³ We also emphasize that while in the Milky Way it might be plausible that a population of HVCs may be missed if these have low velocities, this is not the case for M31 or M33 where “HVCs” with any velocities (included systemic velocities of M31 and M33) can be clearly spatially separated from the galaxy.

6 SUMMARY

In this work we have built on the results presented by LH11 and reported on the covering factors and distances of the HVCs, as well as the associations of HVCs observed in H I 21-cm emission with those found in absorption. We emphasize that the UV absorption diagnostics are much more sensitive to low column density gas than H I emission (or optical absorption diagnostics such as Ca II; e.g., Richter et al. 2011). This allows us to probe clouds over several orders of magnitude in H I column density, from $N(\text{H I}) < 10^{15} \text{ cm}^{-2}$ to $N(\text{H I}) > 10^{20} \text{ cm}^{-2}$. We are also able to probe a wide range of ionization conditions and densities because we use several species in different ionization stages (e.g., O I, C II, C IV, Si II, Si III, Si IV). We summarize the results of our study as follows:

(i) With a carefully-selected, large sample of AGN that cover the sky at $|b| \gtrsim 20^\circ$, we find that the covering factor of the HVCs with $|v_{\text{LSR}}| \geq 90 \text{ km s}^{-1}$ of the entire Galactic sky is $68\% \pm 4\%$. About 74% of the HVC directions have $N(\text{H I}) < 3 \times 10^{18} \text{ cm}^{-2}$ and 46% have $N(\text{H I}) < 8 \times 10^{17} \text{ cm}^{-2}$ from a comparison of our results with 21-cm H I emission surveys.

(ii) The full sample of AGN and a sample with more uniform and higher S/N data gives the same covering factor. HVCs with a total H column density $N(\text{H}) < 10^{17} (Z/Z_\odot)^{-1} \text{ cm}^{-2}$ are unlikely to play an important role in the total mass of the HVCs. However, HVCs with $N(\text{H I}) \ll 10^{17} \text{ cm}^{-2}$ are not rare and have still significant mass in view of the detections of metal ion absorption.

(iii) With the distance, position, and velocity information, we unambiguously associate the denser (H I emission selected) and more diffuse (UV absorption selected) regions of HVCs. We argue that most of the predominantly neutral HVC complexes have ionized envelopes that extend beyond the H I contours and that the predominantly ionized HVCs contain at least as much mass as the H I component. However, there are also large regions of Galactic sky that are filled with ionized high-velocity gas with little evidence for H I counterparts nearby. One such region is found toward the Galactic center and may be generated by Galactic outflows.

(iv) The covering factors of HVCs with $90 \leq |v_{\text{LSR}}| \lesssim 170 \text{ km s}^{-1}$ determined from the AGN and LH11 stellar samples are very similar. This confirms that HVCs are within 5–15 kpc of the sun. The HVCs are therefore flows of gas in the inner Milky Way halo. Our new results also show that the covering factor of HVCs drops with decreasing z , which is consistent with theoretical predictions of HVCs falling onto the Milky Way disk. The HVCs are far enough to have a substantial mass ($M \propto d^2$), but are also near enough to be able to reach the disk. They are therefore the most likely source of gas required to support continued star formation in the Milky Way.

(v) While there is no large disparity in the covering factor of the HVCs between the two Galactic hemispheres, the situation is very different for the VHVCs (HVCs with $|v_{\text{LSR}}| > 170 \text{ km s}^{-1}$). At $b > 0^\circ$, the covering of the VHVC is only 13%, but at $b < 0^\circ$, 46% of the Galactic sky is covered by VHVCs. Most of the VHVCs are associated with the Magellanic Stream at $b < 0^\circ$; a large fraction also appears to

be related to the leading arm of the Stream (possibly even at higher positive latitude than previously thought). Other VHVCs with $170 \lesssim |v_{\text{LSR}}| \lesssim 210 \text{ km s}^{-1}$ are affiliated with complex A, C, and the anti-center complex.

(vi) All these elements strongly suggest that in our Local Group of galaxies there is no evidence that HVCs are found much beyond 50 kpc from their host galaxy, except for structures that are directly related to galaxy interaction (like the Magellanic Stream). However, compact VHVCs may have been mostly missed along pencil-beam sightlines; these compact HVCs are the only remaining HVC candidates for dark matter mini-halos.

ACKNOWLEDGMENTS

We thank Bart Wakker for useful discussions. Support for this research was provided by NASA through grants HST-GO-11592.01-A, HST-GO-11598.01, and HST-GO-11741.01-A from the Space Telescope Science Institute, which is operated by the Association of Universities for Research in Astronomy, Incorporated, under NASA contract NAS5-26555. All of the data presented in this paper were obtained from the Multi-mission Archive at the Space Telescope Science Institute (MAST). STScI is operated by the Association of Universities for Research in Astronomy, Inc., under NASA contract NAS5-26555. This research has made use of the NASA Astrophysics Data System Abstract Service and the SIMBAD database, operated at CDS, Strasbourg, France.

APPENDIX A: DISTANCE OF HVC COMPLEXES

We discuss below the connection or absence of connection between the HVCs seen in absorption toward the stars from the LH11 sample (and one additional star HD195455) and in H I emission.

– *NGC5904-ZNG1*: No high-velocity H I emission is observed along this sightline, which is not surprising as Zech et al. (2008) derived $\log N(\text{H I}) = 16.5$ using the Lyman series. The HVCs at $v_{\text{LSR}} = -140, -120 \text{ km s}^{-1}$ have similar velocities as those observed in complex L seen several degrees away (for more information and the spectra, see Zech et al. 2008). Complex L and this star are in the general direction of the Galactic center where lie also the stars NGC6723-III60 (negative latitude) and PG1323-086 (positive latitude). Toward these stars, high-velocity absorption is observed at about -90 km s^{-1} (see Fig. 9 and Table 5), but they are not close to any known H I HVC complex. Similarly, AGN and deep H I observations also show additional HVCs at both negative and positive velocities toward the Galactic center (Keeney et al. 2006; Lockman et al. 2002). It would be interesting to map out the entire region of the Galaxy center with deep H I and H α observations at $|v_{\text{LSR}}| > 90 \text{ km s}^{-1}$ to determine the extent of the ionized gas in this region and its possible connection with complex L. The HVCs observed toward NGC5904-ZNG1 have a very well determined metallicity based on O I and H I absorption, which is super-solar ($[\text{O}/\text{H}] = +0.22 \pm 0.10$). (Another test for the connection or not of these clouds with complex L would be to measure the

metallicity of complex L). In similar directions, O VI absorption is also detected at these positive and negative velocities closer to the plane (e.g., toward HD168941, see Bowen et al. 2008), so these HVCs could be affiliated with flows originating in the disk. The super-solar metallicity, large column of predominantly ionized gas seen in the direction of the inner Galaxy, presence of both positive and negative velocity may suggest that they participate to a galactic fountain fed by outflows occurring in the central regions of the Milky Way.

– *M13-Barnard29*: An HVC is observed in absorption at -121 km s^{-1} (see the spectra in Welsh et al. 2011). The sightline passes near to (but outside of) the H I contours of complex C and no LAB H I emission is observed at -121 km s^{-1} . However, the absorption velocity is similar to velocities observed in the nearby H I emission from complex C. The distance of complex C was derived to be at $d = 10 \pm 2.5 \text{ kpc}$ (Thom et al. 2008, and see also Wakker et al. 2007). While the distance of M13-Barnard29, 7.1 kpc, is slightly outside this distance bracket, it is not inconsistent, especially taken into account a 10% error on the distance of M13-Barnard29, possible variation in the distances of complex C with position, and similarity in the velocities. Therefore this sightline probably traces the extended ionized envelope of complex C. We therefore disagree with the conclusions of Welsh et al. (2011) who argued that the distance of this star was too small for the gas to be associated with complex C.

– *HD195455*: This star lies in the general direction of the IVC complex gp, which spans LSR velocities between $+55$ and $+90 \text{ km s}^{-1}$. The HVC observed at $+95 \text{ km s}^{-1}$ toward this direction could be a higher velocity extended ionized component of this complex. The IVC Complex gp component is also observed at $+70 \text{ km s}^{-1}$ along this sightline (see Fig. 11). The distance of HD195455 is consistent with the bracketed distance of complex gp between 1.8 and 3.8 kpc (Wakker et al. 2008).

– *HS1914+7139*: Two HVCs were detected along this sightline at $v_{\text{LSR}} = -118, -175 \text{ km s}^{-1}$, which are associated with the Outer Arm and/or complex C (see for more information and the spectra in Lehner & Howk 2010, and also discussion in Tripp & Song 2012). LAB H I emission was detected only in the -112 km s^{-1} component.

– *PG0122+214*: This line of sight has also two HVCs detected in absorption at -91 and -160 km s^{-1} (see Fig. 9) and passes near the anti-center HVC complexes, more specifically near the Cloud WW507 and the Cohen stream, where similar velocities are observed. Again no high-velocity H I emission is observed along this sightline. The distance of PG0122+214 (9.6 kpc) is consistent with the bracket distance of 5–11.7 kpc derived by Wakker et al. (2008). However, the higher velocity component was not observed in the stellar spectra of Wakker et al. (2008), so this star places a new upper limit to the distance of the higher velocity gas observed in this complex.

– *PG0832+675*: This line of sight differs with the others in the sense that H I emission is observed with the peak emission centered at -145 km s^{-1} , which is different from the observed absorption centered at -123 km s^{-1} . In Fig. 10, we show the LAB H I 21-cm emission and the normalized spectra of O I, C II, Al III, Si II, S II, and Fe II. The central velocities of the low and intermediate velocity components seen in S II absorption and H I emission are the same, and therefore the difference between the absorption and emis-

sion at high velocities is real. Although the UV spectrum is complicated by many stellar features, the component at -123 km s^{-1} is very likely interstellar because the velocity is the same for different species (C II, O I, N I, Si II, Fe II, although we note that O I and N I are likely contaminated at -123 km s^{-1}) and different from the star (-70 km s^{-1}), and because the column densities derived from different transitions of the same species give the same values ($\log N(\text{Fe II}) = 12.65 \pm 0.02$ based on the $\lambda 2344, 2382$ transitions and $\log N(\text{Al III}) = 12.55 \pm 0.05$ based on the $\lambda 1854, 1862$ transition, and $\log N(\text{Si II}) = 13.00 \pm 0.08$ based on the $\lambda 1193, 1260, 1304$ transitions).

PG0832+675 lies in the direction of complex A within the H I contour, so it is not surprising to see H I emission in this direction. The star is likely at the front edge of complex A, which would explain why the O I is so weak at -145 km s^{-1} (the metallicity of complex A –B.P. Wakker, private communication 2011 – would imply a far stronger absorption). Wakker (2001) summarized a distance bracket for this complex of 4.0–9.9 kpc (see Wakker et al. 1996; van Woerden et al. 1999). Given that we see little O I, C II, Si II, and Fe II absorption at -145 km s^{-1} toward PG0832+675 compared to the H I column density at the same velocity, we conclude that most of the H I lies behind the star. This implies a distance bracket for the predominantly neutral gas of complex A of 8.1–9.9 kpc. The -123 km s^{-1} component may be the ionized envelope of complex A or an unrelated foreground cloud. The upper limit for its distance, in either case, is thus 8.1 kpc. While Barger et al. (2012) observed H α emission in complex A at LSR velocities ranging from -220 to -110 km s^{-1} , there is no strong evidence of H α emission at -123 km s^{-1} over a 1° beam toward this star (K. Barger 2011, private communication). This does not rule out that the -123 km s^{-1} component is part of complex A.

– *PG1002+506*: The H I HVC WW503 is about 2.5° away from this sight line with $v_{\text{LSR}} = -105 \text{ km s}^{-1}$ (B.P. Wakker, private communication 2011), similar to the velocity observed in absorption. Our observations provide a new upper limit, $< 13.9 \text{ kpc}$, on the distance to the ionized component of this cloud. This strongly suggests that most of the HVCs in the anti-center region at $b < 0^\circ$ are within about 10 kpc (see Wakker et al. 2008). On the other hand, no H I emission is observed near this direction at $v_{\text{LSR}} = +101 \text{ km s}^{-1}$, indicating the presence of a positive velocity HVC that is not associated with a H I complex at a distance $d < 13.9 \text{ kpc}$.

– *PG0855+294*: Several small high-velocity H I clouds are observed in this general direction. This sightline passes 0.5° away from HVC WW113 seen in H I emission at $v_{\text{LSR}} = -90 \text{ km s}^{-1}$ (B.P. Wakker, private communication 2011), setting an upper limit of 6.5 kpc for the extended ionized component of these clouds.

– *PG0914+001*: This sightline is near complex WA ($v_{\text{LSR}} = +140$ – $+170 \text{ km s}^{-1}$) and WB ($v_{\text{LSR}} = +80$ – $+110 \text{ km s}^{-1}$), and absorption features at $+110$ and $+170 \text{ km s}^{-1}$ are observed in the spectrum of this star (for more information and the spectra, see LH11). This places an upper limit of 16 kpc for the extended ionized envelope of these HVCs. For the WB complex, the HVCs could be closer as Thom et al. (2006) derived a bracket distance of 7.5–11.1 kpc.

– *EC10500-1358*: This sightline is also in the general direction of complex WA, but the velocity seen in absorption

($v_{\text{LSR}} = +97 \text{ km s}^{-1}$, see the spectra in Fig. 9) is smaller. It is, however, about 0.5° from HVC WW95 at $v_{\text{LSR}} = +100 \text{ km s}^{-1}$, setting a distance limit of 5.2 kpc for this cloud.

– *NGC104-UIT14*: This sightline shows no HVC absorption, although it has strong H I 21-cm emission observed at $+112 \text{ km s}^{-1}$, with a H I column density $\log N(\text{H I}) = 20.39$. This sightline passes in the southern part of the WE complex (Morras et al. 2000; Wakker 2001), which is a patchy ensemble of HVCs at similar velocities rather than a large continuous structure like complex C. The limit from O I gives $\log N(\text{O I}) < 13.8$ at 3σ . It is unlikely that the metallicity in this complex is $< 0.5 \times 10^{-3} Z_\odot$, implying that the star sets a lower limit on the distance of WE, and hence using the upper limit from Sembach, Savage, & Massa (1991), the WE complex is at $4.5 < d < 12.8 \text{ kpc}$.

REFERENCES

- Barger K. A., Haffner L. M., Wakker B. P., Hill A. S., Madsen, G.J., Duncan A.K., 2012, ApJ, submitted
- Benjamin R. A., Danly L., 1997, ApJ, 481, 764
- Besla G., Kallivayalil N., Hernquist L., van der Marel R. P., Cox T. J., Kereš D., 2012, MNRAS, 2457
- Bland-Hawthorn J., Sutherland R., Agertz O., Moore B., 2007, ApJ, 670, L109
- Blitz L., Spergel D. N., Teuben P. J., Hartmann D., Burton W. B., 1999, ApJ, 514, 818
- Bouché N., Lehnert M. D., Aguirre A., Péroux C., Bergeron J., 2007, MNRAS, 378, 525
- Bowen D. V., et al., 2008, ApJS, 176, 59
- Braun R., Thilker D. A., 2004, A&A, 417, 421
- Bregman J. N., 1980, ApJ, 236, 577
- Brüns C., et al., 2005, A&A, 432, 45
- Charlton J. C., Churchill C. W., Rigby J. R., 2000, ApJ, 544, 702
- Chiappini C., Matteucci F., Romano D., 2001, ApJ, 554, 1044
- Chomiuk L., Povich M. S., 2011, AJ, 142, 197
- Churchill C. W., Mellon R. R., Charlton J. C., Jannuzi B. T., Kirhakos S., Steidel C. C., Schneider D. P., 2000, ApJ, 543, 577
- Collins J. A., Shull J. M., Giroux M. L., 2003, ApJ, 585, 336
- Collins J. A., Shull J. M., Giroux M. L., 2005, ApJ, 623, 196
- Collins J. A., Shull J. M., Giroux M. L., 2009, ApJ, 705, 962 [CSG09]
- Dekel A., et al., 2009, Nature, 457, 451
- Ferland G. J., Korista K. T., Verner D. A., Ferguson J. W., Kingdon J. B., Verner E. M., 1998, PASP, 110, 761
- Fitzpatrick E. L., Spitzer L., Jr., 1997, ApJ, 475, 623
- Fox A. J., Savage B. D., Wakker B. P., 2006, ApJS, 165, 229
- Fox A. J., Savage B. D., Wakker B. P., Richter P., Sembach K. R., Tripp T. M., 2004, ApJ, 602, 738
- Fox A. J., Wakker B. P., Savage B. D., Tripp T. M., Sembach K. R., Bland-Hawthorn J., 2005, ApJ, 630, 332
- Fox A. J., Wakker B. P., Smoker J. V., Richter P., Savage B. D., Sembach K. R., 2010, ApJ, 718, 1046
- Fraternali F., Binney J. J., 2006, MNRAS, 366, 449
- Fumagalli M., Prochaska J. X., Kasen D., Dekel A., Ceverino D., Primack J. R., 2011, MNRAS, 418, 1796
- Ganguly R., Sembach K. R., Tripp T. M., Savage B. D., 2005, ApJS, 157, 251
- Giovanelli R., Haynes M. P., Kent B. R., Adams E. A. K., 2010, ApJ, 708, L22
- Gnat O., Sternberg A., 2004, ApJ, 608, 229
- Green J. C., et al., 2012, ApJ, 744, 60
- Harris W. E., 1996, AJ, 112, 1487
- Harris W. E., 2010, arXiv, arXiv:1012.3224
- Heitsch F., Putman M. E., 2009, ApJ, 698, 1485
- Hill A. S., Haffner L. M., Reynolds R. J., 2009, ApJ, 703, 1832
- Joung M. R., Bryan G. L., Putman M. E., 2012, ApJ, 745, 148
- Kalberla P. M. W., Burton W. B., Hartmann D., Arnal E. M., Bajaja E., Morras R., Pöppel W. G. L., 2005, A&A, 440, 775
- Keeney B. A., Danforth C. W., Stocke J. T., Penton S. V., Shull J. M., Sembach K. R., 2006, ApJ, 646, 951
- Kereš D., Hernquist L., 2009, ApJ, 700, L1
- Kereš D., Katz N., Weinberg D. H., Davé R., 2005, MNRAS, 363, 2
- Kwak K., Henley D. B., Shelton R. L., 2011, ApJ, 739, 30
- Lehner N., Keenan F. P., Sembach K. R., 2001, MNRAS, 323, 904
- Lehner N., Howk J. C., 2007, MNRAS, 377, 687
- Lehner N., Howk J. C., 2010, ApJ, 709, L138
- Lehner N., Howk J. C., Science, 334, 955 [LH11]
- Lehner N., Staveley-Smith L., Howk J. C., 2009, ApJ, 702, 940
- Lehner N., Zech W. F., Howk J. C., Savage B. D., 2011, ApJ, 727, 46
- Leitner S. N., Kravtsov A. V., 2011, ApJ, 734, 48
- Lockman F. J., Murphy E. M., Petty-Powell S., Urlick V. J., 2002, ApJS, 140, 331
- Marinacci F., Fraternali F., Nipoti C., Binney J., Ciotti L., Londrillo P., 2011, MNRAS, 415, 1534
- Meiring J. D., et al., 2011, ApJ, 732, 35
- Moehler S., Heber U., 1998, A&A, 335, 985
- Morras R., Bajaja E., Arnal E. M., Pöppel W. G. L., 2000, A&AS, 142, 25
- Murphy E. M., Lockman F. J., Savage B. D., 1995, ApJ, 447, 642
- Nidever D. L., Majewski S. R., Burton W. B., 2008, ApJ, 679, 432
- Oort J. H., 1970, A&A, 7, 381
- Oppenheimer B. D., Davé R., Kereš D., Fardal M., Katz N., Kollmeier J. A., Weinberg D. H., 2010, MNRAS, 406, 2325
- Peek J. E. G., Putman M. E., Sommer-Larsen J., 2008, ApJ, 674, 227
- Prochaska J. X., Hennawi J. F., 2009, ApJ, 690, 1558
- Putman M. E., 2006, ApJ, 645, 1164
- Putman M. E., et al., 1998, Nature, 394, 752
- Putman M. E., et al., 2009, ApJ, 703, 1486
- Putman M. E., Bland-Hawthorn J., Veilleux S., Gibson B. K., Freeman K. C., Maloney P. R., 2003, ApJ, 597, 948
- Putman M. E., Saul D. R., Mets E., 2011, MNRAS, 418, 1575
- Ramspeck M., Heber U., Moehler S., 2001, A&A, 378, 907

- Ribaudo J., Lehner N., Howk J. C., Werk J. K., Tripp T. M., Prochaska J. X., Meiring J. D., Tumlinson J., 2011, *ApJ*, 743, 207
- Richter P., Charlton J. C., Fangano A. P. M., Bekhti N. B., Masiero J. R., 2009, *ApJ*, 695, 1631
- Richter P., Krause F., Fechner C., Charlton J. C., Murphy M. T., 2011, *A&A*, 528, A12
- Ringwald F. A., Rolleston W. R. J., Saffer R. A., Thorstensen J. R., 1998, *ApJ*, 497, 717
- Rolleston W. R. J., et al., 1997, *MNRAS*, 290, 422
- Rolleston W. R. J., Hambly N. C., Keenan F. P., Dufton P. L., Saffer R. A., 1999, *A&A*, 347, 69
- Ryans R. S. I., Keenan F. P., Sembach K. R., Davies R. D., 1997, *MNRAS*, 289, 83
- Savage B. D., et al., 2000, *ApJS*, 129, 563
- Sembach K. R., Savage B. D., Lu L., Murphy E. M., 1995, *ApJ*, 451, 616
- Sembach K. R., Savage B. D., Lu L., Murphy E. M., 1999, *ApJ*, 515, 108
- Sembach K. R., Savage B. D., Massa D., 1991, *ApJ*, 372, 81
- Sembach K. R., et al., 2000, *ApJ*, 538, L31
- Sembach K. R., et al., 2003, *ApJS*, 146, 165
- Shapiro P. R., Field G. B., 1976, *ApJ*, 205, 762
- Smoker J. V., Fox A. J., Keenan F. P., 2011, *MNRAS*, 415, 1105
- Shull J. M., Stevans M., Danforth C., Penton S. V., Lockman F. J., Arav N., 2011, *ApJ*, 739, 105
- Shull J. M., Jones J. R., Danforth C. W., Collins J. A., 2009, *ApJ*, 699, 754
- Steidel C. C., Sargent W. L. W., 1992, *ApJS*, 80, 1
- Thilker D. A., Braun R., Walterbos R. A. M., Corbelli E., Lockman F. J., Murphy E., Maddalena R., 2004, *ApJ*, 601, L39
- Thom C., Peek J. E. G., Putman M. E., Heiles C., Peek K. M. G., Wilhelm R., 2008, *ApJ*, 684, 364
- Thom C., Putman M. E., Gibson B. K., Christlieb N., Flynn C., Beers T. C., Wilhelm R., Lee Y. S., 2006, *ApJ*, 638, L97
- Thom C., Werk J. K., Tumlinson J., Prochaska J. X., Meiring J. D., Tripp T. M., Sembach K. R., 2011, *ApJ*, 736, 1
- Tripp T. M., Jenkins E. B., Bowen D. V., Prochaska J. X., Aracil B., Ganguly R., 2005, *ApJ*, 619, 714
- Tripp T. M., et al., 2011, *Science*, 334, 952
- Tripp T. M., Song L., 2012, *ApJ*, 746, 173
- Tripp T. M., et al., 2003, *AJ*, 125, 3122
- Tumlinson J., et al., 2011, *Science*, 334, 948
- van Woerden H., Schwarz U. J., Peletier R. F., Wakker B. P., Kalberla P. M. W., 1999, *Nature*, 400, 138
- Wakker B. P., 2001, *ApJS*, 136, 463
- Wakker B. P., 1991, *A&A*, 250, 499
- Wakker B. P., et al., 1999, *Nature*, 402, 388
- Wakker B. P., et al., 2003, *ApJS*, 146, 1
- Wakker B. P., et al., 2007, *ApJ*, 670, L113
- Wakker B., Howk C., Schwarz U., van Woerden H., Beers T., Wilhelm R., Kalberla P., Danly L., 1996, *ApJ*, 473, 834
- Wakker B. P., van Woerden H., 1991, *A&A*, 250, 509
- Wakker B. P., van Woerden H., 1997, *ARA&A*, 35, 217
- Wakker B. P., York D. G., Wilhelm R., Barentine J. C., Richter P., Beers T. C., Ivezić Ž., Howk J. C., 2008, *ApJ*, 672, 298
- Welsh B. Y., Wheatley J., Lallement R., 2011, *PASP*, 123, 914
- Westmeier T., Braun R., Thilker D., 2005, *A&A*, 436, 101
- Westmeier T., Brüns C., Kerp J., 2008, *MNRAS*, 390, 1691
- Yao Y., Shull J. M., Danforth C. W., 2011, *ApJ*, 728, L16
- Zech W. F., Lehner N., Howk J. C., Dixon W. V. D., Brown T. M., 2008, *ApJ*, 679, 460

This paper has been typeset from a \LaTeX file prepared by the author.